*horticulturae*

MDPI

*Article*

# Analysis of the Origin of Lilac Fragrance: Insights from Volatile Metabolomics and Transcriptomics

**Ya Tuo [1], Xinying Wei [1], Xuyang Dai [1], Peng Xie [2], Shulan Bai [1], Yu-e Bai [1,*] and Wenquan Bao [1,*]**

[1] College of Forestry, Inner Mongolia Agricultural University, Hohhot 010018, China; tuoya5639502@163.com (Y.T.); wxy0968@163.com (X.W.); dxy20000320@163.com (X.D.); baishulan2017@126.com (S.B.)
[2] Landscape Architecture Construction Service Center of Hohhot, Hohhot 010000, China; asgaze420@gmail.com
* Correspondence: bye666@163.com (Y.-e.B.); ndbwq@imau.edu.cn (W.B.)

## Abstract

Lilac (*Syringa oblata* Lindl.) is an important eco-economic aromatic shrub in northern China; however, the key volatile organic compounds (VOCs) responsible for its floral aroma and their origin remain largely unexplored. In this study, we conducted an integrated analysis of volatile metabolomics and transcriptomics to elucidate the composition, dynamic changes, and potential regulatory network of VOCs across different floral organs and petal developmental stages. A total of 1440 VOCs were identified in the stamens, pistils, and petals, with petals being the primary contributors to the overall floral aroma. Analysis of different petal developmental stages revealed that the full-bloom stage (S3) is critical for VOCs emission. The floral aroma of *S. oblata* is primarily composed of terpenoids, alcohols, and aldehydes. By relative odor activity value (rOAV) with multivariate statistical screening, seven key VOCs with high contributions to the floral aroma were identified. Transcriptome analysis identified 69,935 differentially expressed genes (DEGs) across petal developmental stages, which were predominantly enriched in metabolic pathways and the biosynthesis of secondary metabolites. The expression patterns of these DEGs were highly consistent with the accumulation trends of VOCs, increasing at stages S2 and S3 and subsequently declining at stage S4. Integrative analysis of VOCs and gene expression further identified candidate genes significantly correlated with the key aroma volatiles. Specifically, the carotenoid pathway-related genes *CYP97A3* and *LYC* may influence the formation of carotenoid-derived volatiles and floral aroma. Additionally, genes associated with the fatty acid-lipoxygenase pathway, transport-related genes, and transcription factors are potentially involved in the formation and regulation of aldehyde and alcohol volatiles. These findings advance our understanding of the floral aroma formation in *S. oblata* and provide metabolic basis, candidate gene resources and a theoretical foundation for the genetic improvement of aroma traits and the breeding of new cultivars.

**Keywords:** *Syringa oblata*; floral aroma; petal; volatile organic compounds; HS-SPME-GC-MS; terpenoid biosynthesis

Check for updates

Academic Editor: Jiafu Jiang

Received: 12 May 2026
Revised: 22 June 2026
Accepted: 29 June 2026
Published: 2 July 2026

**Copyright:** © 2026 by the authors. Licensee MDPI, Basel, Switzerland. This article is an open access article distributed under the terms and conditions of the Creative Commons Attribution (CC BY) license.

## 1. Introduction

Floral aroma is a complex chemical signal formed by VOCs emitted from plants, primarily consisting of low molecular weight volatile terpenoids, phenylpropanoids/benzenoids, and fatty acid derivatives [1]. These compounds facilitate plant adaptation to environmental conditions and are implicated in regulating reproductive processes and stress

responses [2,3]. The VOCs that produce fragrance exert multiple beneficial effects on the human body, exhibiting pharmacological activities such as stimulating cranial nerves, dilating cardiovascular and cerebrovascular systems, sedative-hypnotic effects, and anticancer properties [4]. Plant VOCs also possess important environmental purification functions, such as disinfection and sterilization, ozone removal, and settling particulate matter [5]. Furthermore, they have potential value in stress relief and adjunctive disease therapy, and can also be used in perfumery and pharmaceuticals. Among them, terpenoids exhibit structural and functional diversity, displaying pronounced biological and pharmacological activities [6], whereas phenylpropanoids/benzenoids and fatty acid derivatives often impart pleasant odors that can evoke positive emotions [7]. Recent research advances have integrated headspace volatile collection techniques with multi-omics approaches to elucidate the biosynthetic pathways and regulatory mechanisms of key VOCs in ornamental plants [8]. However, significant differences in the synthesis and regulation of VOCs persist across different species and even cultivars, highlighting the ample scope for further research in this field.

The emission of floral VOCs exhibits distinct organ and spatiotemporal specificity. In lotus (*Nelumbo nucifera*), the stamen is the principal organ for aroma emission, where the rOAV of terpenoids and esters is significantly higher than in petals and carpels, and its VOCs peak on the day of flowering and the following day, forming a strong sweet and fruity character [1]. In *Cymbidium tracyanum*, the dynamic patterns of terpenoids vary considerably across flower developmental stages and among different floral parts, with the flower base and lip recognized as key regions for aroma emission [2]. These studies indicate that floral aroma formation relies not only on the accumulation of VOCs in specific organs but is also closely related to their developmental stages.

Terpenoids represent the largest class of VOCs, whose biosynthesis proceeds through the mevalonate (MVA) and the 2-C-methyl-D-erythritol-4-phosphate (MEP) pathways [3]. Phenylpropanoids and benzenoids typically originate from the phenylalanine pathway within the cytosol, whereas fatty acid derivatives are produced in chloroplasts through fatty acid oxidation [9]. In recent years, using multi-omics technologies, such as transcriptomics and metabolomics, researchers have deeply elucidated the biosynthetic mechanisms of these VOCs in plants including Wintersweet (*Chimonanthus praecox*) [10], kiwifruit (*Actinidia chinensis*) [11], lotus (*Nelumbo nucifera*) [1], Tracy's Cymbidium (*Cymbidium tracyanum*) [2], and carnation (*Dianthus caryophyllus*) [12].

*S. oblata* is a deciduous shrub or small tree in the family *Oleaceae* and represents an important aromatic woody species [13]. This species is distinguished by luxuriant foliage, elegant flower color, an early flowering period, intense fragrance, and pronounced tolerance to drought, cold, and saline-alkaline soils. Valued not only for its ornamental qualities, *S. oblata* can also be processed into essential oils, perfumes, and pharmaceuticals, making it a shrub of significant economic value in northern China. In other *Oleaceae* plants, β-ionone and linalool are the main VOCs in sweet osmanthus (*Osmanthus fragrans*) [14]. Benzyl acetate, linalool, isoeugenol, and (3E,6E)-α-farnesene are the key VOCs in jasmine (*Jasminum sambac*), and they belong to the classes of volatile terpenoids and volatile phenylpropanoids/benzenoids [15]. The emission characteristics of VOCs vary markedly among species and cultivars within the genus *Syringa*. *Syringa* × *persica* 'Alba-variegata' exhibited the highest VOCs emission rate, reaching 1.8 times that of *Syringa meyeri* 'Si Ji Lan'; a total of 80 VOCs were detected across several lilac species, which were categorized into nine groups including benzenoids, terpenoids, alcohols, and aldehydes, among which six components such as ethylbenzene, m-xylene, and *p*-xylene were identified as common high-abundance substances [12]. Notable compositional differences were observed between species: *Syringa vulgaris* 'Alba' was dominated by terpenoids (e.g., β-ocimene), whereas

*Syringa* × *persica* 'Alba-variegata' and *Syringa velutina* showed the highest proportions of benzenoids. Among the cultivars examined, *S. oblata*, white lilac (*S. oblata var. alba*), and red lilac (*Syringa villosa*) are all dominated by esters and alkanes, with white lilac presenting the highest relative content of esters (e.g., benzyl acetate) and red lilac containing more organic acids (e.g., benzoic acid); *Syringa* reticulata is characterized by furfural (28.5%) and phenethyl alcohol (15.2%), contributing to its distinct sweet aroma [16].

This study employed an integrated approach utilizing headspace solid-phase microextraction (HS-SPME), gas chromatography–mass spectrometry (GC–MS), and transcriptome sequencing (RNA-Seq). This methodology enabled the identification of VOCs emitted from different floral tissues of *S. oblata* and the analysis of their dynamic changes during flowering. Furthermore, by combining metabolomic and transcriptomic data, we elucidated the biosynthetic pathways underlying the characteristic floral VOCs of *S. oblata* and identified the floral organs responsible for lilac fragrance. Collectively, these analyses provide novel insights into the formation and compositional features of floral aroma volatiles in this species.

From a horticultural perspective, the expected results have several practical applications. The clarification of VOC composition and its dynamic changes during flowering provides a scientific basis for optimizing harvest timing and selecting appropriate floral tissues for cut flowers, landscape display, or natural fragrance extraction. Identifying the specific floral organs that contribute most to lilac fragrance can guide targeted cultivation and variety selection to enhance aromatic performance in gardens. The integrated metabolomic and transcriptomic framework established here offers a reference for studying floral aroma traits in other ornamental horticultural plants, supporting efforts to improve aroma quality, pollinator attraction, and overall ornamental value.

## 2. Materials and Methods

### *2.1. Plant Materials*

Sampling was conducted at the Arboretum in Hohhot, Inner Mongolia Autonomous Region, China (40°48′ N, 111°42′ E). From late April to early May 2025, healthy, pest-free branches of *S. oblata* growing under natural photoperiod conditions were selected. Petals, pistils, and stamens were collected for tissue-specific VOCs analysis. Each tissue was sampled in triplicate, with consistent sampling time and quantity to minimize experimental variation. To capture the dynamic changes in floral aroma profiles and biosynthesis mechanisms, petal samples were collected across four developmental stages: bud (Stage 1, S1), opening (Stage 2, S2), full-bloom (Stage 3, S3), and late flowering (Stage 4, S4). Pistils (S3-S) and stamens (S3-Pi) were collected at the full-bloom stage (S3). Following collection, all samples were snap-frozen in liquid nitrogen and stored at −80 °C until analysis.

In the experiment, 30 flowers were randomly selected. Petal length was measured using a vernier caliper, and petal color was assessed using the RHS (Royal Horticultural Society) color chart. Additionally, intact flowers at each developmental stage were collected, weighed for fresh weight, then dried at 65 °C to constant weight, and the dry weight was recorded to calculate the dry-to-fresh weight ratio.

### *2.2. Sample Preparation and GC-MS Acquisition Conditions for VOCs*

The petals, stamens and pistils of floral tissues were ground into homogeneous powder. A 0.5 g aliquot was transferred into a 20 mL headspace vial containing 2 mL saturated NaCl solution (Agilent, Palo Alto, CA, USA) fitted with TFE-silicone headspace septa (Agilent) to inhibit enzymatic activity. Volatiles were captured via an automated PAL RSI (Robotic Sample Injection) system (CTC Analytics AG, Zwingen, Switzerland) and analyzed by GC-MS.

HS-SPME: Sample vial equilibrated at 60 °C with agitation for 5 min; 120 µm DVB/CWR/PDMS fiber (2 cm length, Agilent Technologies, Santa Clara, CA, USA) exposed to headspace at 60 °C for 15 min, thermally desorbed at 250 °C for 5 min (GC injector). Fiber pre-conditioned at 250 °C for 5 min before use to avoid carryover [17].

GC condition: Analysis was performed on an Agilent 8890 gas chromatograph and an Agilent 7000D triple quadrupole mass spectrometer (Agilent Technologies, Santa Clara, CA, USA); DB-5MS column (30 m × 0.25 mm × 0.25 µm); carrier gas (helium ≥ 99.999%), flow rate 1.2 mL $min^{-1}$, injector 250 °C (split mode, split ratio 5:1), solvent delay 3.5 min. Oven program: 40 °C (3.5 min) → 100 °C (10 °C $min^{-1}$) → 180 °C (7 °C $min^{-1}$) → 280 °C (25 °C $min^{-1}$, 5 min). MS condition: EI ionization (70 eV), ion source 230 °C, quadrupole 150 °C, transfer line 280 °C; SIM mode (per GB 23200.8-2016) [18], for each compound, one quantitative ion and two to three qualitative ions were set for precise scanning [19,20].

### *2.3. Qualitative and Quantitative Analysis of VOCs*

A custom volatile database was established by integrating multiple resources, including the Metware self-built database (MWDB, Wuhan Metware Biotechnology Co., Ltd., Wuhan, China), literature reports, partial reference standards, and retention indices. The MWDB is a specialized volatile metabolomics database constructed based on over 200 plant species, more than 500 authentic standards, and over 300 published literature reports, covering more than 5000 volatile compounds in plants (including terpenoids, esters, aldehydes, ketones, alcohols, aromatic hydrocarbons, acids, amines, ethers, nitrogen/sulfur-containing compounds, and heterocyclic compounds). Qualitative analysis was performed using Agilent MassHunter Qualitative software (14.0) with deconvolution parameters set at a peak width of 20, and the requirements for resolution, sensitivity, and peak shape were all set to medium. Compound identification was carried out by comparing the obtained mass spectra with the NIST (2020) library and the MWDB. The minimum match factor was set at 700. Meanwhile, the retention index (RI) of each volatile compound was calculated using a mixture of n-alkanes (C7–C40) (purchased from O2Si Specialty Products, Rochester, NY, USA, catalog No. CDGG-110219-06) as a standard under the same GC-MS conditions, and the RI values were compared with literature values with an acceptable criterion of RIi ± 30, calculated according to Van Den Dool and Kratz (1963): RI = 100Z + 100[TR(x) − TR(z)]/[TR(z + 1) − TR(z)], where TR(x), TR(z), and TR(z + 1) are the retention temperatures of the target component and n-alkanes with carbon numbers Z and Z + 1, respectively, and TR(z) < TR(x) < TR(z + 1). Importantly, all compounds matched to the MWDB carry additional confidence due to database-level authentic standard validation. Compounds whose RT and characteristic fragment ions met the parameter settings were considered target compounds (GB 23200.8-2016) [21,22].

For the quantitative analysis of VOCs, a semi-quantitative internal standard method was employed. Prior to sample extraction, an appropriate amount of the isotopically labeled internal standard, 3-Hexanone-2,2,4,4-$d_4$ (CDN Isotopes, Shanghai, China, catalog No. D-8095-0.5g), was precisely added to each sample. The relative content of each VOC in the solid samples was calculated using the following formula, based on the ratio of the peak area of the target compound to that of the internal standard [23]:

$$X_i = \frac{V_s \times C_s}{M} \times \frac{I_i}{I_s} \times 10^{-3}$$

where $X_i$ represents the content of compound i in the sample (µg/g); $V_s$ is the volume of the internal standard added (µL); $C_s$ is the concentration of the internal standard (µg/mL); $M$ is the mass of the sample (g); $I_i$ is the peak area of compound i in the sample; and $I_s$ is the peak area of the internal standard [24].

### *2.4. Relative Odor Activity Value Analysis of VOCs*

In this study, the relative odor activity value (rOAV) was used to quantitatively evaluate the aroma contribution of each VOCs. rOAV is a classic method established by integrating compound sensory thresholds to identify key VOCs in food, and is used to assess the contribution of each VOC to the overall aroma characteristics of a sample. In recent years, rOAV has been increasingly applied to the screening of key VOCs in various plants. Among all detected VOCs, compounds with rOAV $\geq 1$ were considered potential contributors to the overall floral aroma of *S. oblata*, while those with rOAV $\geq 1000$ were regarded as high-contribution aroma compounds. By further applying multivariate statistical screening criteria (VIP > 1) and fold change (FC < 0.5 or FC > 2), the key VOCs responsible for the floral aroma were ultimately identified from these high-contribution candidates [25–27]. However, rOAV itself only reflects the magnitude of the contribution and does not directly provide the sensory attributes of the compounds. The calculation formula is as follows:

$$\mathrm{rOAV_i} = \frac{\mathrm{C_i}}{\mathrm{T_i}}$$

where $\mathrm{rOAV_i}$ represents the relative odor activity value of compound i, $\mathrm{C_i}$ is the relative content of the compound (μg/g), and $\mathrm{T_i}$ is the threshold value of the compound (μg/g). To assign specific aroma descriptions to each compound, we consulted multiple publicly available databases and published literature. Specifically, the aroma descriptions of the compounds were obtained from http://www.thegoodscentscompany.com, http://perflavory.com/, http://www.odour.org.uk/odour/index.html, http://foodflavorlab.cn/#/home (accessed on 20 June 2025), or from the literature [25–28]. By combining the rOAV values with these aroma descriptors, we were able to infer the sensory attributes of the key VOCs and construct odor radar plots for different floral organs and developmental stages.

### *2.5. RNA Extraction and RNA-Seq Analysis*

Total RNA was extracted, with integrity and concentration assessed using a Qsep400 Bioanalyzer (Bioptic Inc., Taiwan, China) and Qubit 4.0 Fluorometer (Thermo Fisher Scientific, Singapore), respectively. Qualified RNA was used for library construction via mRNA isolation, cDNA synthesis, end repair, A-tailing, adapter ligation, purification, and PCR amplification. Library quality was verified by Qubit quantification, Agilent 2100 Bioanalyzer (Santa Clara, CA, USA) (insert-size), and q-PCR (effective concentration > 2 nM); qualified libraries were processed into DNA nanoballs (DNBs) for high-throughput sequencing. The sequencing platform was DNBSEQ-T7, and the sequencing strategy employed was paired-end 150 bp (PE150).

Eighteen samples (six groups, three biological replicates each) were analyzed. Raw reads were filtered with fastp (removing adapters, reads with >10% N bases, or >50% bases with $Q \leq 20$) to obtain clean data. Trinity software (v2.15.1) was used to perform de novo assembly of the clean data, yielding unigene sequences. To obtain comprehensive functional annotation, the unigene sequences were aligned against multiple public databases: DIAMOND BLASTX was employed to align the unigene sequences against the KEGG, NR, Swiss-Prot, GO, COG/KOG, and TrEMBL databases (E-value $\leq 1 \times 10^{-5}$), while HMMER software was used to search against the Pfam database for protein domain identification. Functional annotation information for the unigenes was obtained by integrating the results from these analyses. Gene expression was quantified as FPKM. Differentially expressed genes (DEGs) were identified with $|\log_2(\text{fold change})| \geq 1$ and FDR < 0.05 (FDR adjusted via Benjamini–Hochberg method), followed by KEGG annotation and enrichment analysis.

### *2.6. Weighted Gene Co-Expression Network Analysis (WGCNA)*

In the WGCNA, the pickSoftThreshold function first calculated the optimal soft-thresholding power (β), applying an RsquaredCut value of 0.85. Next, pairwise gene expression correlations served as the basis for constructing a clustering dendrogram. Finally, gene modules were identified by the dynamic tree cut algorithm, using a merge cut height of 0.25 and a minModuleSize of 50.

### *2.7. Identification of Compound-Related Genes*

To discover potential terpene synthase (TPS) genes in *S. oblata*, a homology-based search strategy was employed. First, known TPS protein sequences from Arabidopsis thaliana, acquired from the TAIR database (https://www.arabidopsis.org/) (accessed on 10 September 2025), served as queries in a BLASTP (2.16.0) analysis against the *S. oblata* proteome, with an E-value cutoff set at $\leq 1 \times 10^{-5}$. The candidate genes thus identified in *S. oblata* were then aligned with their corresponding Arabidopsis sequences. Functional predictions for these candidates were made by interrogating the UniProt database (https://www.uniprot.org/uniprotkb) (accessed on 13 September 2025) and surveying the relevant scientific literature, focusing on genes known to be involved in VOCs biosynthesis.

### *2.8. Statistical Analysis*

Principal Component Analysis (PCA) was performed on the samples to obtain a preliminary understanding of the overall metabolite differences among groups and the degree of variation within each group. The PCA results revealed a separation trend among the groups, indicating whether differences existed in the metabolome within the sample groups [29].

For variables with low inter-sample correlation, orthogonal partial least-squares discriminant analysis (OPLS-DA) and orthogonal signal correction (OSC) were applied. These methods decompose the X-matrix information into two components: one correlated with Y and the other uncorrelated with Y. By removing uncorrelated variations, differential variables were screened. Prior to OPLS-DA, the raw data were $\log_2$ transformed and then mean-centered, where X represented the sample quantitative information matrix and Y the sample grouping information matrix. The analysis was performed using the OPLSR.Anal function in the MetaboAnalystR package of R software to obtain OPLS-DA results. The predictive parameters for evaluating the OPLS-DA model included $R^2X$, $R^2Y$, and $Q^2$. $R^2X$ and $R^2Y$ indicate the proportion of variance explained by the model for the X and Y matrices, respectively, while $Q^2$ represents the predictive ability of the model. The closer these three indicators are to 1, the more stable and reliable the model is. A $Q^2$ value > 0.5 indicates a valid model, and a $Q^2 > 0.9$ indicates an excellent model.

Based on the Variable Importance in Projection (VIP) derived from the OPLS-DA model (with biological replicates $\geq 3$), metabolites that differed significantly between groups were preliminarily screened. In combination with univariate analysis (*p*-value/FDR; biological replicates $\geq 2$) or fold change (FC) values, differential metabolites were further screened. The criteria for screening differential metabolites in this study were: VIP > 1 and fold change $\geq 2$ or fold change $\leq 0.5$, which were considered significantly different.

Differential gene screening was performed using $DESeq^2$ [30,31] for differential expression analysis between sample groups. The input for differential analysis was the raw read counts of genes (non-normalized). After differential analysis, the Benjamini–Hochberg method was used to correct the *p*-values for multiple hypothesis testing, yielding the false discovery rate (FDR). The screening criteria for differentially expressed genes were $|\log_2\text{Fold Change}| \geq 1$ and FDR < 0.05.

KEGG annotation of differential metabolites was performed using the KEGG database (http://www.kegg.jp/kegg/compound/, accessed on 22 September 2025). The annotation results of significantly differential metabolites were classified and displayed, with KEGG pathway classification information obtained from the KEGG database.

## 3. Results

### *3.1. Phenotypic Characteristics of Floral Organs of S. oblata*

At stage S1, the flower buds were closed, the corolla was not exposed or only slightly exposed, petal length $\leq$ 0.4 cm, the angle between adjacent sepals < 15°, color was N79 D Moderate Reddish Purple, fresh weight of the flower was 5 mg, dry weight 1 mg, and dry-to-fresh weight ratio 20%. At stage S2, the corolla lobes were loose and displayed an erect to semi-expanded posture, petal length 0.5–0.6 cm, opening angle between 20° and 50°, the basal color appeared as 84 B Light Purple, fresh weight 8 mg, dry weight 1.2 mg, dry-to-fresh weight ratio 15%. At stage S3, morphological characteristics of the three floral organs were observed: petals were fully horizontally expanded, ovate in shape, with entire margins, glabrous surface, length $\geq$ 0.6 cm, opening angle $\geq$ 70°, flower color reached maximum saturation (75 B Light Purple), fresh weight of petals was 12 mg, dry weight 1.4 mg, dry-to-fresh weight ratio 12%; the anthers were approximately 2 mm long, filaments approximately 6 mm long, anthers pale yellow; the pistil had a bifid stigma, style length approximately 3 mm, ovary diameter approximately 2 mm. At stage S4, brown necrotic spots appeared on the petal margins, tissues lost water and wilted, no stable geometric features of length or angle could be determined, or petals had already abscised; fresh weight of the flower bud was 10 mg, dry weight 1.4 mg, dry-to-fresh weight ratio 14% (Figure 1).

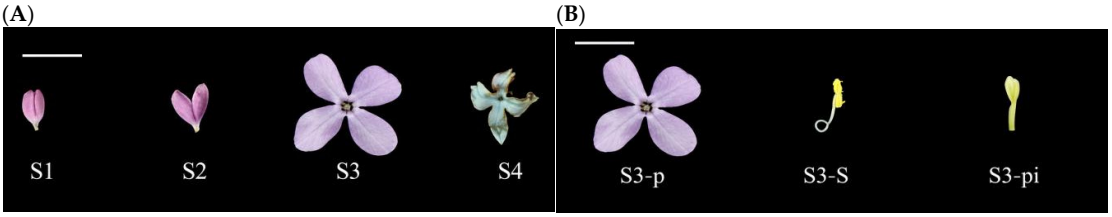



**Figure 1.** Phenotype of floral organs in *S. oblata*. (**A**) Petal phenotype at different developmental stages. bud stage (S1), opening stage (S2), full-bloom stage (S3), and late flowering stage (S4). (**B**) Floral organ phenotype at full-bloom stage. Petal (S3-p), Pistil (S3-s) and stamen (S3-pi). scale bar: 1 cm.

### *3.2. GC-MS Identification Results*

Through comprehensive GC-MS analysis, a total of 1440 volatile organic compounds VOCs were identified from the floral organs (petals, stamens, and pistils) of *S. oblata* (Supplementary Table S1). These compounds were classified into 15 chemical categories: acids, alcohols, aldehydes, amines, aromatics, esters, ethers, halogenated hydrocarbons, heterocyclic compounds, nitrogen-containing compounds, ketones, hydrocarbons, phenols, sulfur-containing compounds, and terpenoids. Internal standard semi-quantification revealed that terpenoids (19.6%), esters (18.07%), ketones (11.4%), alcohols (10.7%), and heterocyclic compounds (9.45%) were the major VOC categories (Figure 2A).

The relative content of each chemical category differed significantly among the three floral organs. Petals exhibited the highest total VOC accumulation (Figure 2B). Specifically, alcohols were most abundant in petal tissues, while terpenoids and esters were relatively enriched in stamens, and ketones showed higher levels in pistils. These organ-specific distribution patterns revealed correlations between compounds and floral organs: alcohols

were mainly associated with petals, terpenoids and esters with stamens, and ketones with pistils.

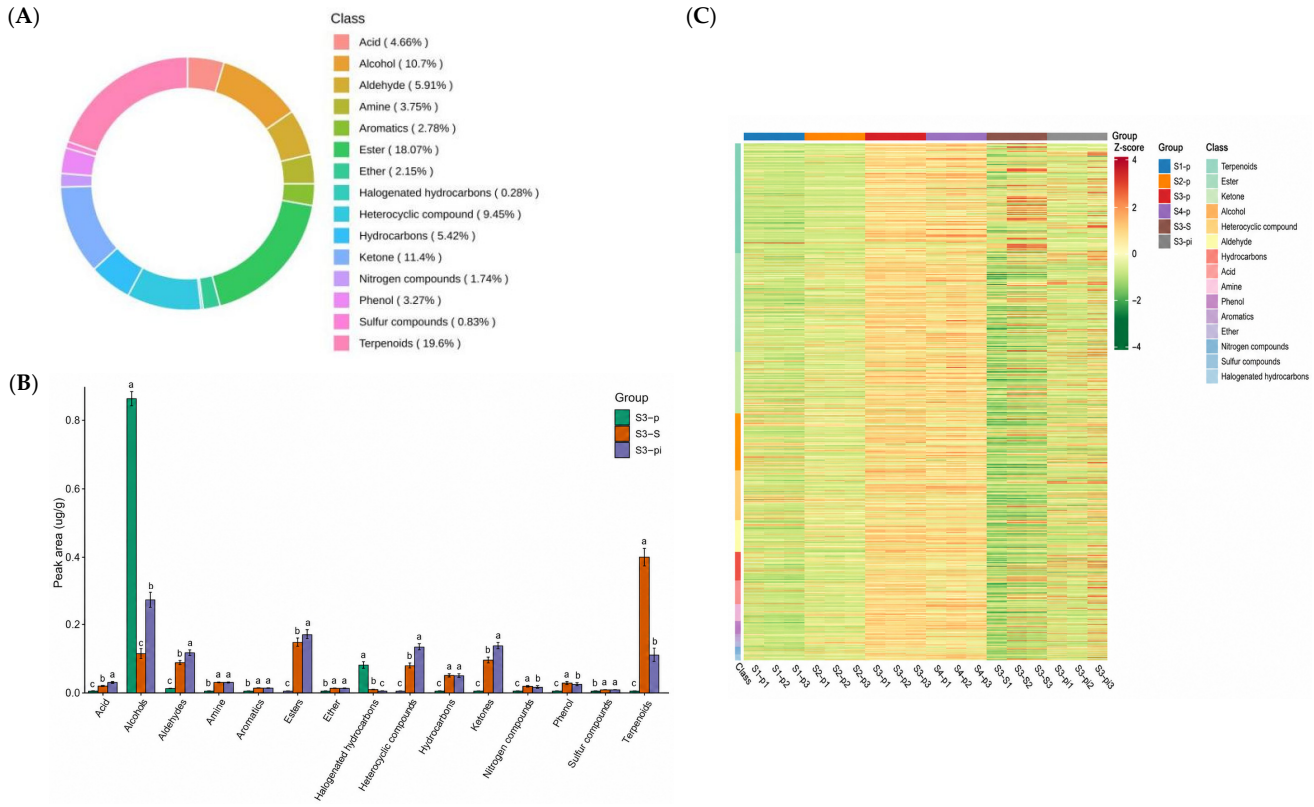



**Figure 2.** Identification and classification of VOCs in different floral organs of *S. oblata*. (**A**) Classification and proportion of VOCs detected in *S. oblata*. (**B**) Total relative concentrations of different groups of volatile organic compounds in each floral organ. (**C**) VOCs clustering heatmap. Note: The horizontal axis represents sample names, and the vertical axis represents metabolite information. "Group" indicates the sample grouping. Different colors represent different values obtained after normalization of relative contents (red indicates high content, green indicates low content).

The Z-score-based heatmap (Figure 2C) further illustrated the dynamic changes in compound categories across different flowering stages and floral organs. During flower development, the relative abundances of terpenoids and esters peaked at stage S3, followed by S2, and were lowest at S1 and S4, which is consistent with the perception of the strongest lilac fragrance at full bloom. Alcohols and aldehydes remained at relatively high levels at both S2 and S3. Heterocyclic compounds and sulfur-containing compounds slightly increased at S4, which may be associated with the production of specific odors during flower senescence. Hydrocarbons and acids exhibited relatively minor changes throughout the flowering period.

### *3.3. Analysis of PCA and OPLS-DA*

Principal component analysis (PCA) further clearly separated the Samples from different floral organs and different developmental stages of petals, with PC1 and PC2 explaining 40.17% and 28.71% of the total variance, respectively (Figure 3), indicating that different floral organs and developmental stages of petals possess specific volatile profiles.

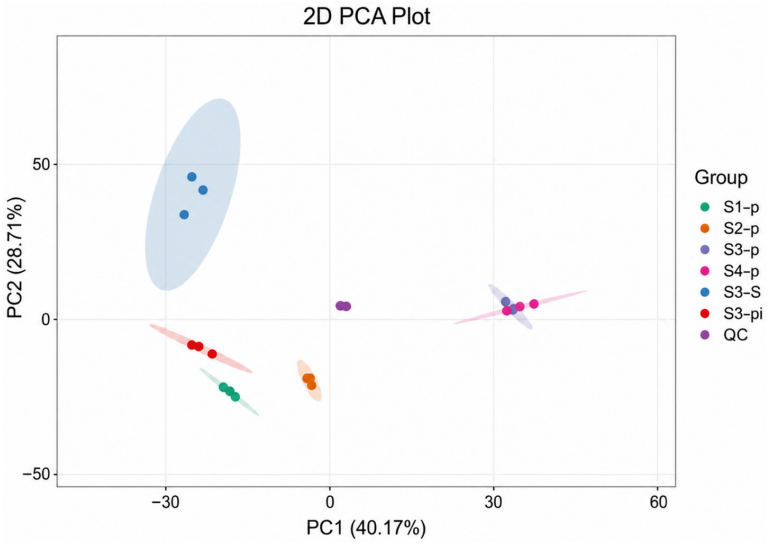



**Figure 3.** PCA plot of different stages of petals and floral organs. Note: PC1 represents the first principal component, PC2 represents the second principal component, and the percentages indicate the proportion of variance in the dataset explained by each principal component. Each point in the figure represents a sample, and samples from the same group are shown in the same color. "Group" denotes the grouping.

To evaluate the reliability and potential overfitting of each OPLS-DA model, 200 random permutation tests were performed for each comparison group. The results are shown in Figure 4 (corresponding to each comparison).

Comparisons of different floral organs: The OPLS-DA models for pistil vs. petal, stamen vs. petal, and pistil vs. stamen all passed the permutation test. The $Q^2$ values of the random permutation models were consistently much lower than the original $Q^2$ values, and the $Q^2$ intercepts were negative, confirming significant metabolic differences among floral organs and robust predictive ability of the models.

Comparisons of different petal developmental stages: The OPLS-DA models comparing the bud, opening, and late flowering stages with the full-bloom stage all passed the permutation test. In each case, the original $Q^2$ value was significantly higher than those of the random permutation models, and the $Q^2$ regression intercept was negative (<0.05), indicating no overfitting and reliable discrimination of metabolic features across developmental stages.

In summary, all OPLS-DA models passed the permutation test without overfitting, and they can be used for subsequent differential metabolite screening.

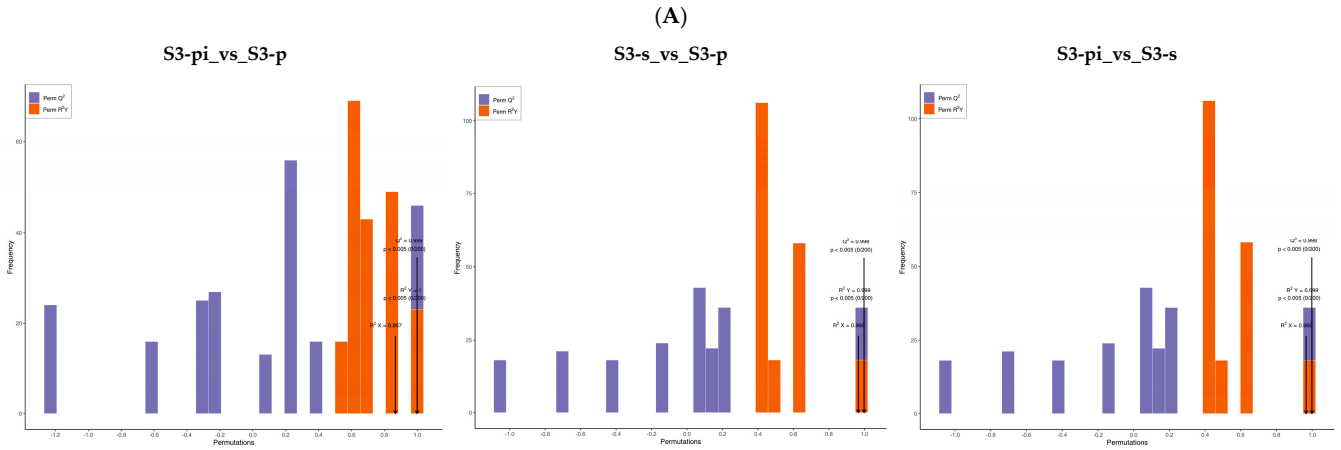



**Figure 4.** *Cont.*

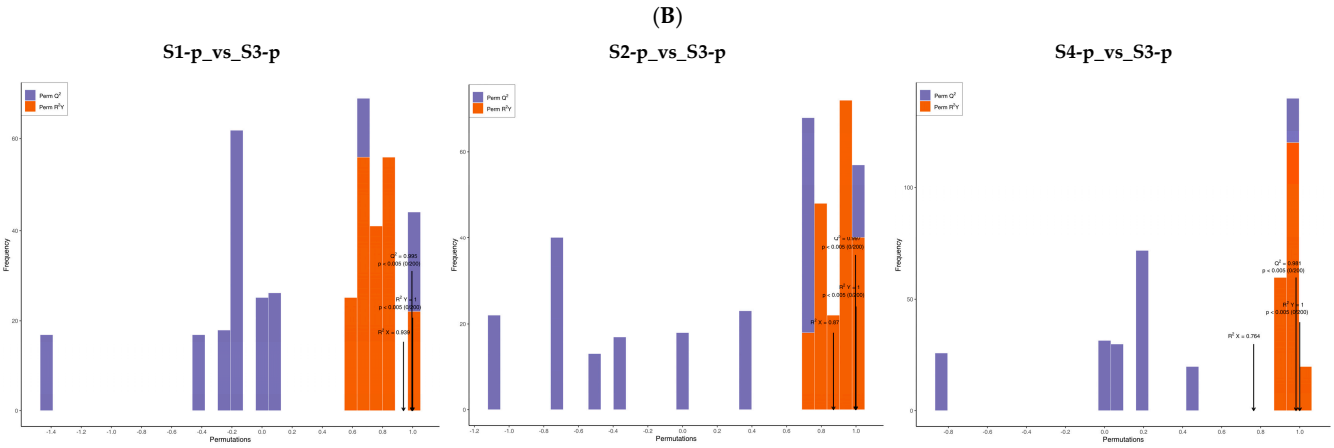



**Figure 4.** Validation of the OPLS-DA model. (**A**) OPLS-DA model validation between floral organs; (**B**) OPLS-DA model validation between floral stages. Note: The x-axis represents the $R^2Y$ and $Q^2$ values of the model, and the y-axis represents the frequency of occurrence of model classification performance in 200 random permutation experiments. In the figure, orange represents $R^2Y$ of the random grouping model, purple represents $Q^2$ of the random grouping model, and the values indicated by the black arrows are the $R^2X$, $R^2Y$, and $Q^2$ values of the original model.

### *3.4. Differential VOCs Analysis Among Floral Organs*

Further pairwise comparisons identified a large number of DAVs: 931, 841, and 782 DAVs in stamen vs. petal, pistil vs. petal, and stamen vs. pistil comparisons, respectively (Figure 5A). In the comparisons using petals as a reference, the number of upregulated DAVs was significantly higher: 759 upregulated and 140 downregulated in petals compared with stamens; 656 upregulated and 160 downregulated in petals compared with pistils, indicating that petals possess a stronger enrichment characteristic in volatile profile composition.

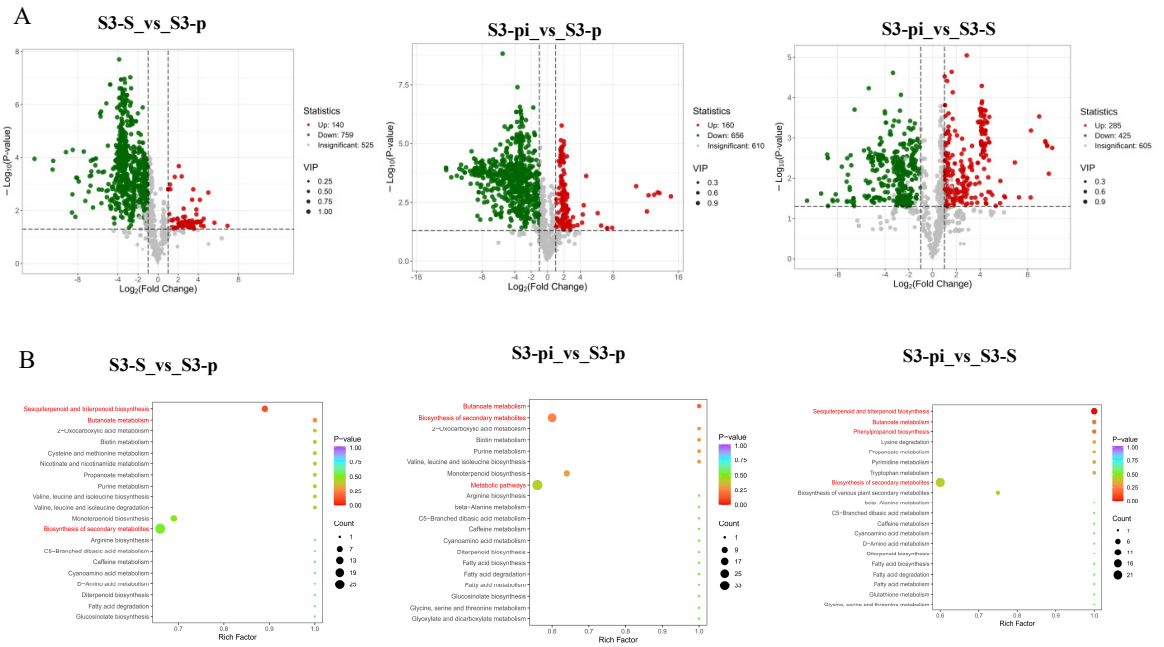



**Figure 5.** Comparative analysis of DAVs in different floral organs of *S. oblata*. (**A**) Volcano plots of differential compounds in each comparison group. (**B**) KEGG analysis of differential compounds in each group.

Based on KEGG database enrichment analysis, many of the DAVs in these floral organs were found to be associated with volatile organic compound biosynthetic pathways.

The key enriched pathways included terpenoid biosynthesis, butanoate metabolism, and biosynthesis of secondary metabolites (Figure 5B). These pathways support the formation of lilac fragrance-related volatiles from different perspectives. Plant floral VOCs are typically composed of multiple classes of secondary metabolites, including terpenoids, phenylpropanoids/benzenoids, fatty acid derivatives, and amino acid derivatives [32]. Among these, terpenoid volatiles constitute an important component of floral aroma in lilac and many aromatic plants. Butanoate metabolism is associated with the formation of volatile ester aromas. The sweet, fruity, and fatty notes in many floral and fruit scents originate from fatty acid-derived aldehydes, alcohols, and esters [33]. Enrichment of the butanoate metabolism pathway may indicate the involvement of short-chain fatty acids and their acyl donors in the formation of potential ester volatiles [34]. These pathways do not independently determine floral aroma but collectively support the biosynthetic background of lilac floral VOCs from the perspectives of terpenoids, fatty acid derivatives, and general secondary metabolism.

Overall, the floral fragrance volatiles of *S. oblata* exhibit organ specificity, with petals contributing the most to the overall volatile profile. This provides a solid metabolic basis for subsequent screening of key metabolites and candidate genes associated with the characteristic floral aroma of *S. oblata*, supporting the contribution of the floral organ level to floral aroma biosynthesis.

### *3.5. Aroma Attribute Identification in S. oblata Flowers*

Odor profile assessment of DAVs in each comparison group was conducted to further delineate the aroma characteristics of different floral organs in *S. oblata*. Overall, the floral aroma of *S. oblata* is primarily characterized by fruity, sweet, and green notes (Figure 6A). Among the organs, DAVs associated with petals exhibited a more prominent contribution to these aroma attributes. Across all comparison groups, 295 DAVs corresponding to these three aroma attributes were identified, with their relative abundance in petals being generally higher than in stamens and pistils (Figure 6B). Among these DAVs, terpenoids were the most abundant compounds associated with fruity, sweet, and green aromas, comprising 121 terpenoid compounds, highlighting their significant contribution to aroma emission (Supplementary Table S2).

To pinpoint the aroma-active compounds, the rOAV was calculated for VOCs in each floral organ (Supplementary Table S3). Following the established criterion [27], compounds with rOAV $\geq 1$ were defined as contributors to aroma. The petals contained numerous compounds with high rOAV values, which were higher than those in stamens and pistils. This indicates that petals are the major site for accumulation of aroma-active compounds (Figure 7A). In terms of the number of compound types, petals contained the highest number of aroma-active compounds with rOAV $\geq 1$ (258 compounds), higher than stamens (207 compounds) and pistils (196 compounds) (Figure 7B).

These active VOCs were mainly classified into 13 categories, among which terpenoids dominated in all three organs, followed by aldehydes and alcohols (Figure 7C). In terms of overall distribution, compounds with rOAV between 1 and 10 accounted for the highest proportion in all organs (Figure 7B). Furthermore, VOCs with rOAV $\geq 1000$ were defined as key aroma contributors, most of which were detected in petals.

In summary, based on the aroma attribute classification and rOAV assessment results, petals exhibit greater prominence in both the quantity and intensity of key aroma-active compounds, suggesting that they may be the primary organ for the formation and emission of floral aroma volatiles in *S. oblata*.

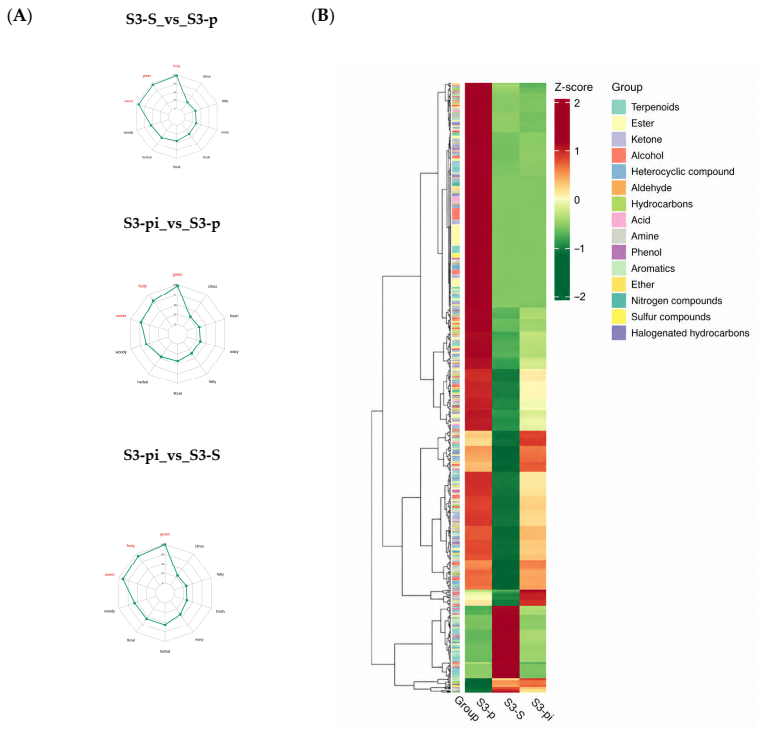



**Figure 6.** Odor profile assessment of DAVs in each comparison group in *S. oblata*. (**A**) Odor characteristics of differential compounds in each group. (**B**) Heatmap analysis of main aroma-producing differential compounds in all comparison groups.

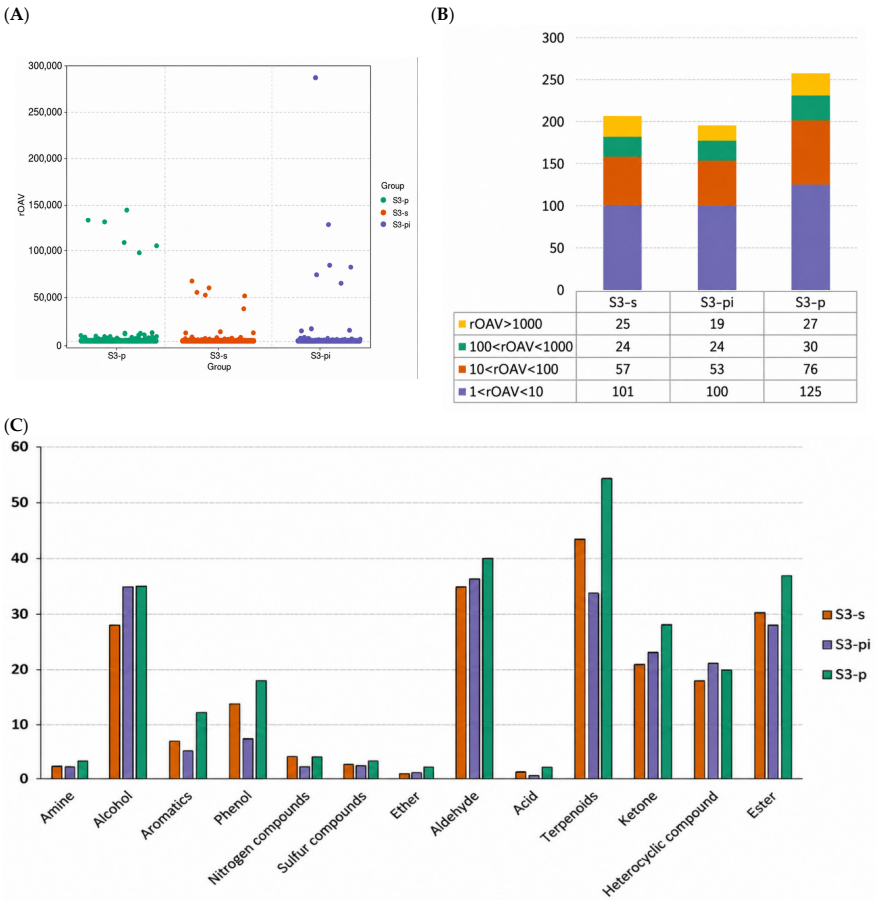



**Figure 7.** Analysis of key aroma compounds in *S. oblata* based on rOAV. (**A**) Scatter plot of rOAV for VOCs in different floral organs. (**B**) Statistical analysis of VOCs with rOAV > 1 in each floral organ. (**C**) Number of vocs with roav > 1 by category in different organs.

### *3.6. VOCs Synthesized in S. oblata Petals During Different Developmental Stages*

A total of 1440 VOCs were detected in petals across the S1–S4 stages, mainly including terpenoids, esters, ketones, alcohols, heterocyclic compounds, and aldehydes. Hierarchical clustering analysis revealed distinct accumulation patterns for VOCs in *S. oblata* petals over the flowering period. A substantial proportion of differential VOCs accumulated prominently at stages S3 and S4 (Figure 8A). From the overall trend of VOCs changes, the major VOCs associated with floral aroma exhibited more pronounced accumulation at the full-bloom stage (S3) (Figure 8B). Petal length, fresh weight, and color saturation all peaked at stage S3, coinciding with an increase in the number of VOCs with rOAV $\geq 1$, suggesting a possible synergistic relationship between petal morphological maturation and aroma emission. Stage S3 represents the most active stage for floral VOCs formation and emission in *S. oblata*.

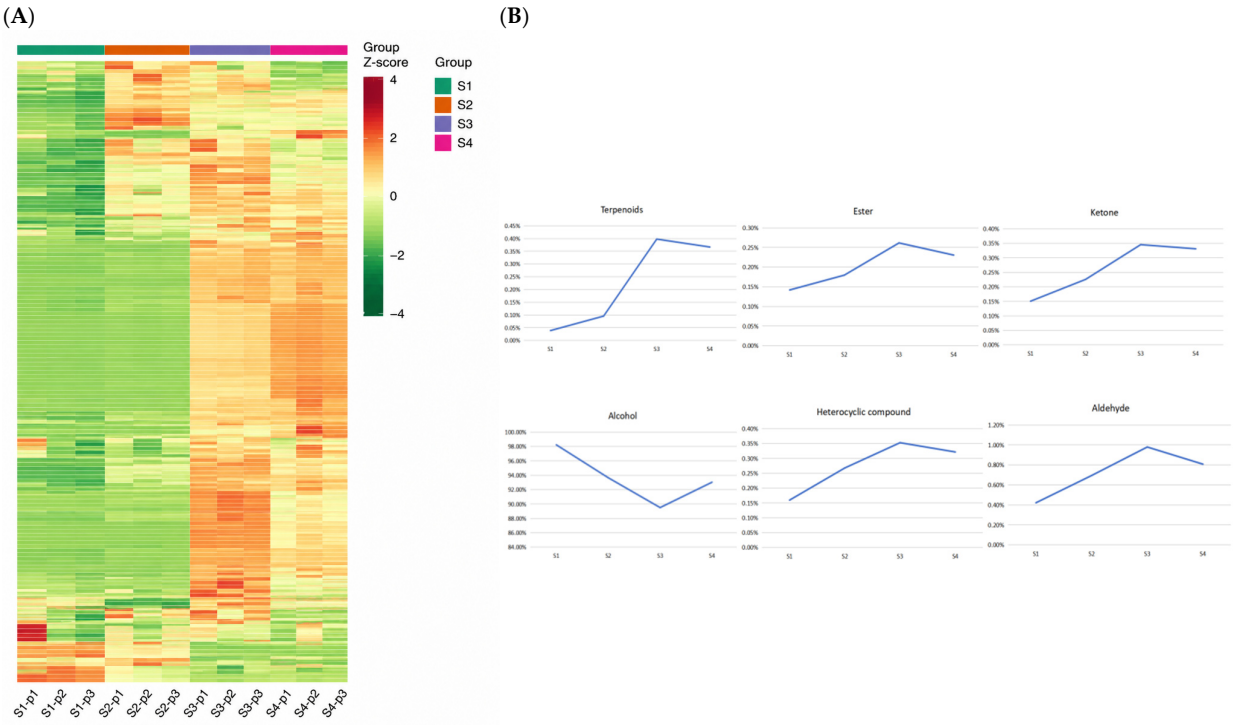



**Figure 8.** Emission of VOCs from petals at different developmental stages. (**A**) Clustered heatmap of VOC content in petals at different developmental stages. (**B**) Dynamic changes in the contents of key VOCs categories.

DAVs analysis showed that, compared with the S3 stage, 100, 54, and 9 VOCs were upregulated at the S1, S2, and S4 stages, respectively (Figure 9A). In comparisons using S4 as a reference, more DAVs were downregulated at the S1 and S2 stages, indicating that the overall volatile profile was weaker in the early flowering stages compared with the later stages, and the difference between S3 and S4 was relatively small. KEGG enrichment analysis of DAVs revealed that they were mainly enriched in metabolic pathways related to volatile formation, including the biosynthesis of secondary metabolites, terpenoid backbone biosynthesis, and sesquiterpenoid and triterpenoid biosynthesis (Figure 9B). Consistent with the volatile composition, aroma attribute analysis indicated that sweet, fruity, and green notes were prominent characteristics of petal aroma during the flowering period (Figure 9C).

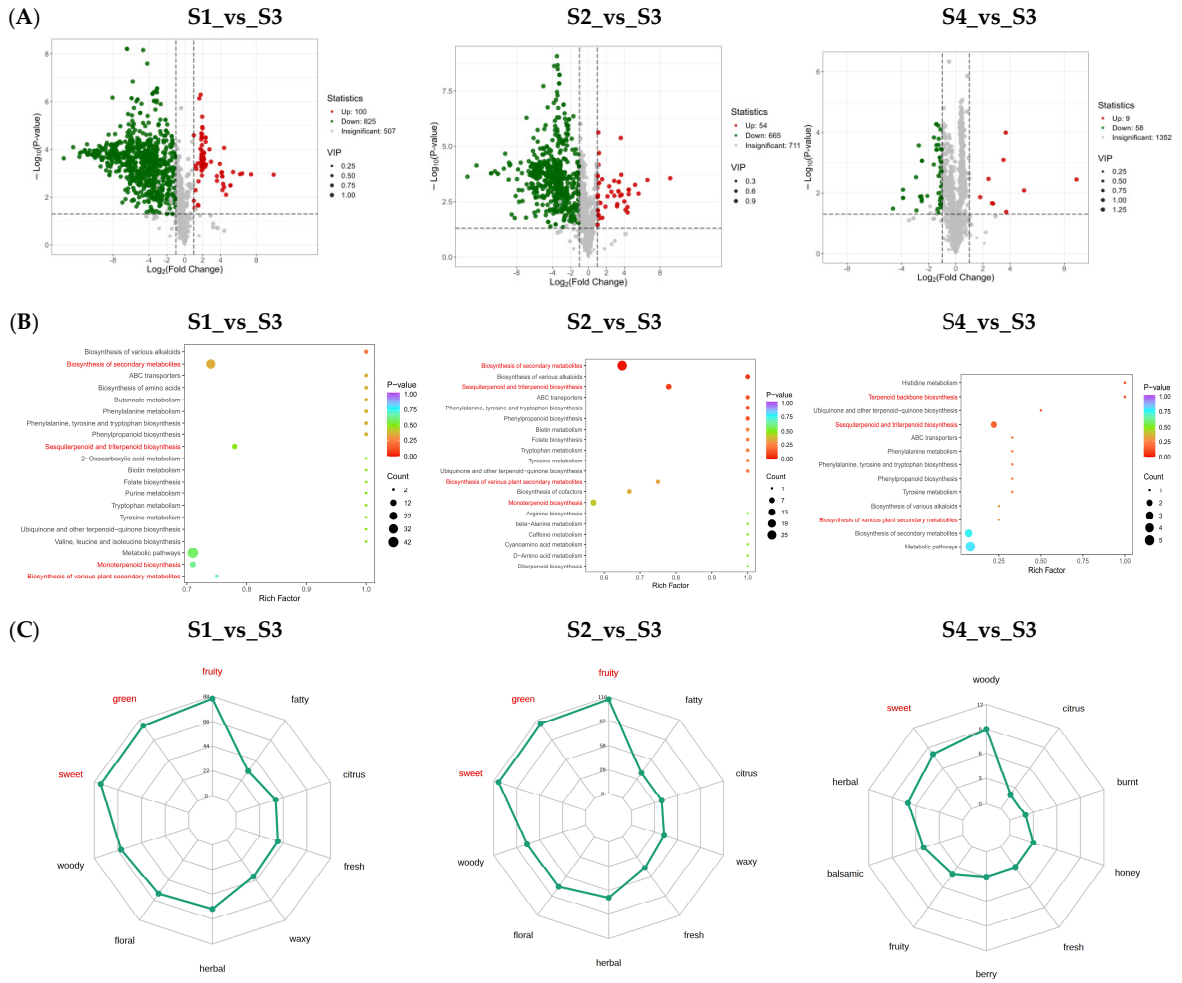



**Figure 9.** Comparative analysis of VOCs in petals at different flowering stages. (**A**) Volcano plot of DAVs in petals at different flowering stages. (**B**) KEGG analysis of DAVs in each group. (**C**) Odor characteristics of differential VOCs in each group.

The rOAV was also determined for petal VOCs across flowering stages. At stage S3, the petals contained numerous compounds with high rOAV values, which were higher than other stages. This indicates that S3 are the major stage for accumulation of aroma-active compounds (Figure 10A). At stages S1, S2, S3, and S4, the numbers of compounds with rOAV $\geq$ 1 were 173, 205, 258, and 254, respectively, reaching the highest level overall at the S3 stage (Figure 10B), indicating that S3 is the critical stage for the formation and emission of strong floral aroma. Further screening for high-contribution compounds with rOAV $\geq$ 1000 identified 27 such compounds at the S3 stage, including aldehydes, alcohols, ketones, esters, heterocyclic compounds, and a small number of terpenoids, among them, the accumulation of terpenoids was highest at the S3 and S4 stages (Figure 10C). Combining the screening criteria of multivariate statistics (VIP > 1) and fold change (FC < 0.5 or FC > 2), we ultimately selected 7 key VOCs (Figure 10D).

Seven VOCs, namely (E)-β-damascone, (E)-2-nonenal, 2-nonenal, (E,Z)-2,6-nonadienal, (E,E)-2,4-nonadienal, α,α,4-trimethyl-3-cyclohexene-1-methanethiol, and (2E,6Z)-2,6-nonadien-1-ol, showed high rOAV values and passed multivariate screening, and were therefore considered the major aroma-active compounds contributing to the characteristic floral aroma of *S. oblata* petals.

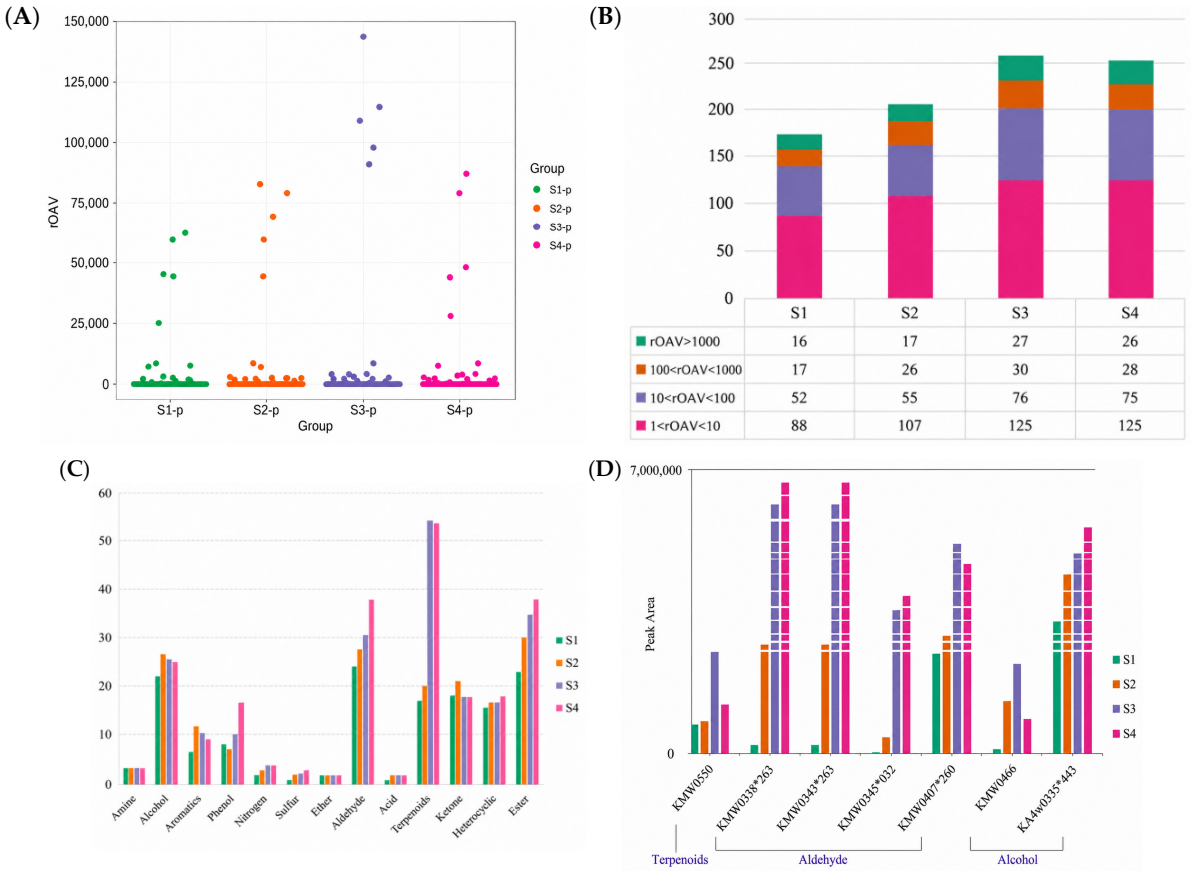



**Figure 10.** Analysis and screening of key aroma compounds based on rOAV in *S. oblata* petals at different flowering stages. (**A**) rOAV scatter plot of VOCs detected in petals at different flowering stages. (**B**) Statistical analysis of VOCs with rOAV > 1 in petals. (**C**) Number of vocs with roav > 1 by category across different petal developmental stages. (**D**) Dynamic changes in content of key VOCs (simultaneously satisfying rOAV > 1000, VIP > 1, and FC < 0.5 or FC > 2) in petals at different developmental stages. Note: KMW0550(β-damascone); KMW0338*263((E)-2-nonenal); KMW0343*263(2-nonenal); KMW0345*032((2E,6Z)-2,6-nonadienal); KMW0407*260((E,E)-2,4-nonadienal); KMW0466(α,α,4-trimethyl-3-cyclohexene-1-methanethiol); KA4w0355*443((2E,6Z)-2,6-nonadien-1-ol).

### *3.7. Transcriptome Characteristics of Petals at Different Developmental Stages and Screening of VOCs-Related Candidate Genes*

We obtained 152.26 Gb of clean data from transcriptome sequencing of 18 samples. Each sample yielded at least 6 Gb of clean data, with a Q30 base percentage ≥ 93%. PCA showed that PC1 and PC2 explained 39.18% and 21.62% of the total variance, respectively, and the samples were clearly classified into four clusters corresponding to flowering stages (Figure 11A), indicating significant differences in the petal transcriptome across different developmental stages.

Across all petal samples, 179,209 genes were quantified. Using S3 as the reference, 50,304, 44,351, and 25,004 DEGs were identified in the S1–S3, S2–S3, and S4–S3 comparisons, respectively (Figure 11B), totaling 69,935 DEGs, among which 11,634 were common to all three comparison groups (Figure 11C). K-means clustering divided the DEGs into seven expression clusters (Figure 11D) (Supplementary Table S4).

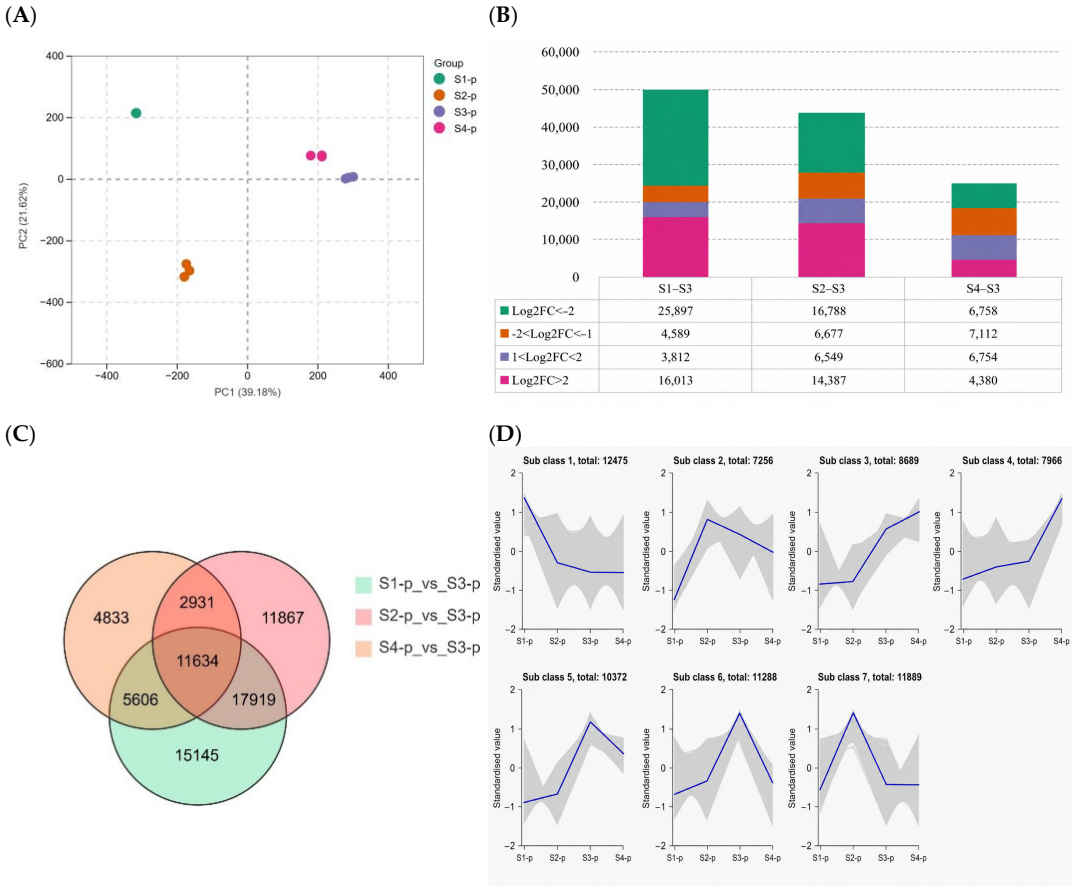



**Figure 11.** Characterization of DEGs in petals during different developmental stages of *S. oblata*. (**A**) PCA of the petal transcriptome data. (**B**) Statistics of DEGs in petals at different developmental stages. (**C**) Venn diagram of DEGs. (**D**) K-means clustering analysis of DEGs.

KEGG enrichment analysis showed that most clusters were significantly enriched in metabolism-related pathways, especially those closely associated with volatile formation such as the biosynthesis of secondary metabolites (Figure 12). Among them, the expression of genes in Cluster 5 and Cluster 6 increased at stages S2–S3 and decreased at stage S4, consistent with the trend of enhanced VOCs at the S3 stage; genes in Cluster 3 were continuously upregulated from S2 to S4, suggesting that they may be related to metabolic processes associated with the late flowering period. Notably, multiple pathways related to VOCs biosynthesis were enriched in different clusters. Cluster 5 and Cluster 6 were enriched in pathways such as fatty acid metabolism, amino acid-related biosynthesis, and carotenoid biosynthesis, while Cluster 3 was enriched in pathways related to terpenoids, phenylpropanoids, and certain fatty acid derivatives, indicating that these DEGs may participate in key metabolic processes involved in volatile formation in *S. oblata* petals.

To further elucidate the transcriptional regulatory patterns associated with VOCs accumulation, WGCNA was performed on the DEGs, and a total of 10 co-expression modules were identified (Figure 13A).

The expression patterns of DEGs differed significantly among these modules. Module-trait correlation analysis showed that the “Turquoise” and “Yellow” modules were significantly positively correlated with 7 key VOCs accumulation, while the “Black” module was significantly negatively correlated with VOCs accumulation (Figure 13B). Combining correlation analysis between key volatiles and modules, and integrating the thresholds of VIP > 1 and $|r| > 0.9$, we selected a set of candidate genes significantly associated with the key VOCs (Table 1).

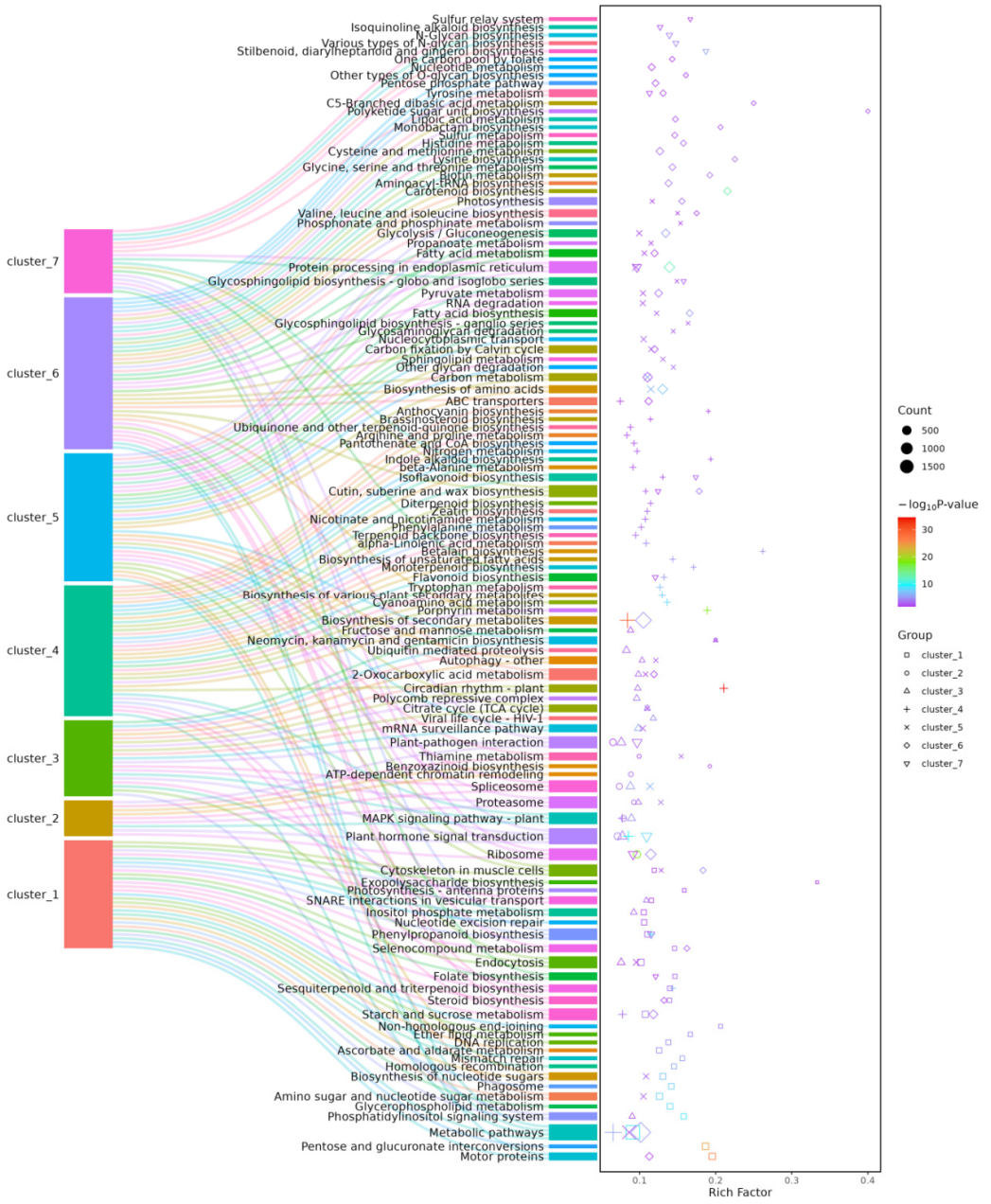



**Figure 12.** Sankey diagram. KEGG pathway annotation of DEGs in each cluster.

Among them, the carotenoid pathway-related genes *CYP97A3* and *LYC* were localized to nodes associated with carotenoid biosynthesis, suggesting that they may be involved in the formation of carotenoid-derived volatiles [35]. Furthermore, genes related to the fatty acid-lipoxygenase pathway and the interconversion of aldehydes and alcohols, such as *KASIII* [36], *FAB2* [37], *FAD2* [38], *FAD8* [9], *LOX6* [39], *CYP74A* [40], and *ADH* [41], were significantly correlated with key aldehydes and alcohols; lipid transfer-related genes *LTPG1* [42] and *LTP4* [43], as well as the transcription factor *WRKY33* [44], were further proposed as potential regulatory candidates, indicating that floral aroma formation in *S. oblata* may be coordinately influenced by the process of "precursor supply—oxidative cleavage and conversion—transport and emission".

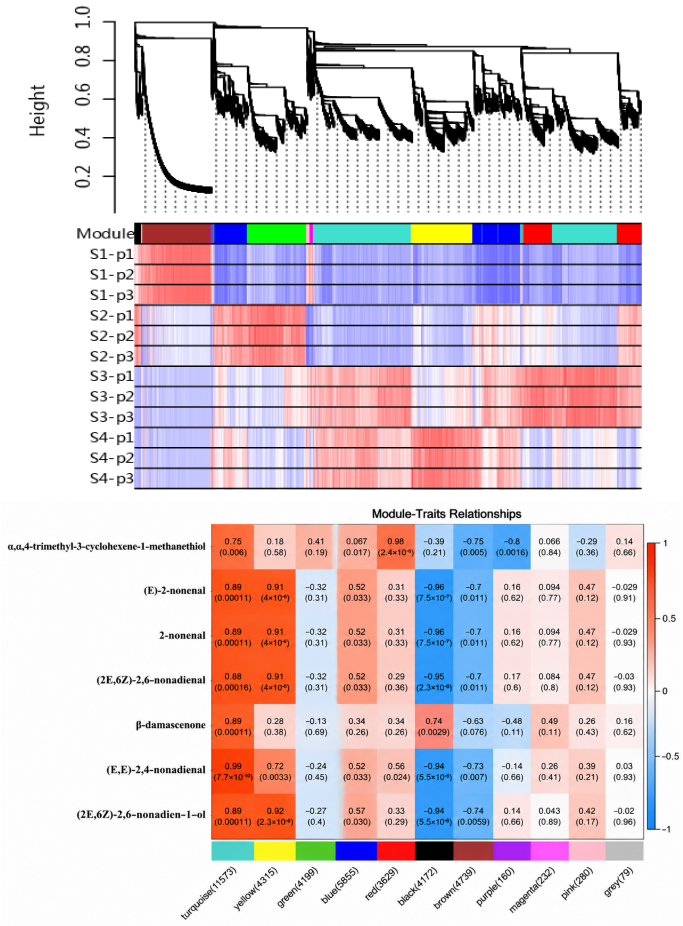



**Figure 13.** WGCNA of petal DEGs and its correlation with key VOCs in *S. oblata* at different developmental stages. (**A**) Hierarchical clustering tree of co-expression modules with DEGs based on WGCNA. Modules were identified based on correlations among gene expression profiles, with a module merging threshold of 0.25 and a minimum module size of 50 genes. Each color represents one co-expression module, in which genes with similar expression patterns may be functionally related. (**B**) Correlation between the 7 key VOCs and the WGCNA modules.

**Table 1.** Summary of candidate genes potentially involved in S. oblata fragrance formation.

| Cluster ID | Gene Name | Putative Function/Pathway | WGCNA Module | Module–VOC Association | Gene–VOC Correlation | Criterion Met | Priority |
|---|---|---|---|---|---|---|---|
| Cluster-71305.7 | *CYP97A3* | Carotenoid biosynthesis | Turquoise | + | β-damascone | √ | **A** |
| Cluster-74692.1 | *LYC* | Carotenoid biosynthesis | Black | - | β-damascone | √ | **A** |
| Cluster-71489.20 | *LTPG1* | GPI-anchored lipid transfer protein 1 | Turquoise | + | alcohols and aldehydes | √ | **B** |
| Cluster-41566.5 | *KAS III* | 3-ketoacyl-ACP synthase III | Turquoise | + | alcohols and aldehydes | √ | **B** |
| Cluster-49252.2 | *LOX6* | lipoxygenase 6 | Turquoise | + | alcohols and aldehydes | √ | **B** |
| Cluster-40083.10 | *WRKY33* | transcription factor WRKY33 | Turquoise | + | alcohols and aldehydes | √ | **B** |
| Cluster-43776.1 | *FAB2* | acyl-[acyl-carrier-protein] desaturase | Turquoise | + | alcohols and aldehydes | √ | **B** |
| Cluster-28963.34 | *FAD2* | fatty acid desaturase 2 | Turquoise | + | alcohols and aldehydes | √ | **B** |
| Cluster-73256.4 | *FAD8* | fatty acid desaturase 8 | Black | - | alcohols and aldehydes | √ | **B** |

**Table 1.** *Cont.*

| Cluster ID | Gene Name | Putative Function/Pathway | WGCNA Module | Module–VOC Association | Gene–VOC Correlation | Criterion Met | Priority |
|---|---|---|---|---|---|---|---|
| Cluster-47988.0 | *Adh* | alcohol dehydrogenase | Turquoise | + | alcohols and aldehydes | √ | **B** |
| Cluster-41071.0 | *CYP74A* | allene oxide synthase | Turquoise | + | alcohols and aldehydes | √ | **B** |
| Cluster-67026.2 | *LTP4* | lipid transfer protein 4 | Turquoise | + | alcohols and aldehydes | √ | **B** |
| Cluster-15259.8 | *ABC1 family protein* | protein associated with volatile compound synthesis | Turquoise | + | β-damascone | √ | **C** |
| Cluster-13652.7 | *EMB1144* | Embryo Defective 1144 | Black | - | β-damascone | √ | **C** |

Note: "+" indicates positive correlation, "-" indicates negative correlation. "√" indicates meeting the screening criteria. A represents strong candidate, B represents medium candidate, and C represents candidate for exploration.

### *3.8. The Carotenoid Biosynthesis Pathway Contributes to Floral Aroma Formation in S. oblata*

Gene function annotation results showed that both candidate genes, *CYP97A3* and *LYC*, are associated with the carotenoid biosynthesis pathway. To visually illustrate their potential metabolic pathways, we constructed a schematic diagram of carotenoid biosynthesis based on the KEGG pathway framework (Figure 14). Combined with the expression profiles at different petal developmental stages, *CYP97A3* and *LYC* showed significant changes at stage S3, the critical period for aroma emission, and their temporal expression patterns were consistent with the variation trends of key VOCs across different flowering stages. Moreover, petal color reached maximum saturation at stage S3, suggesting that the carotenoid pathway may simultaneously influence both flower color and floral aroma in *S. oblata*. Furthermore, in the WGCNA, *CYP97A3* and *LYC* were assigned to co-expression modules significantly associated with VOCs traits and showed significant correlations with the carotenoid-derived VOC β-damascone. Based on comprehensive evidence from pathway annotation, stage-specific expression characteristics, module assignment, and metabolite correlations, *CYP97A3* and *LYC* were considered as primary candidates potentially involved in the floral aroma formation of *S. oblata*.

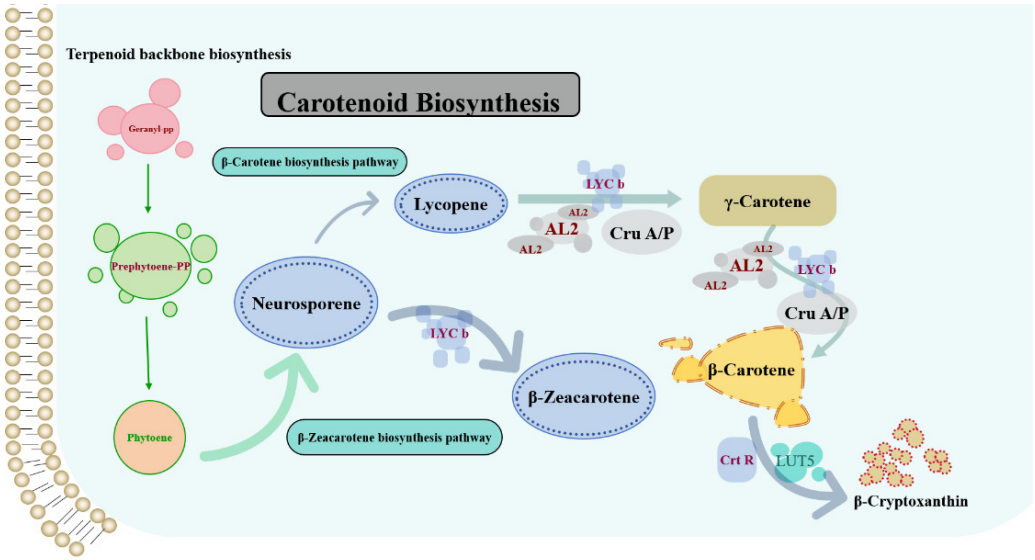



**Figure 14.** Schematic diagram of the carotenoid biosynthesis pathway. Key enzymes and genes, including *LYCb*, *AL2*, *CruA/P*, *CrtR*, and *LUT*, collectively regulate carotenoid biosynthesis.

### *3.9. Correlation Analysis of Key Candidate Genes via WGCNA*

A co-expression network analysis was conducted to clarify the regulatory mechanisms of aroma biosynthesis in *S. oblata* petals during flowering, with a focus on the correlation patterns of the candidate genes *CYP97A3* (carotene β-ring hydroxylase) and *LYC* (lycopene β-cyclase) within their respective WGCNA modules. Based on the WGCNA, together with differential expression analyses among floral organs and developmental stages, 14 candidate genes potentially involved in the biosynthesis of seven key aroma compounds were identified. These genes included *CYP97A3*, *LYC*, *LTPG1*, *KAS III*, *LOX6*, *WRKY33*, *FAB2*, *FAD2*, *FAD8*, *Adh*, *CYP74A*, *LTP4*, *ABC1 family protein*, and *EMB1144*, which showed significant positive or negative correlations with key VOCs, including β-damascone, alcohols, and aldehydes. Among them, *CYP97A3* and *LYC* are associated with carotenoid biosynthesis and showed strong correlations with terpenoid volatiles. *CYP97A3* was assigned to the "Turquoise" module, within which strongly correlated genes were identified, including one encoding an *ABC1 family protein*, which may be associated with VOC biosynthesis. In contrast, *LYC* was assigned to the "Black" module, where it showed high co-expression with *EMB1144* (Embryo Defective 1144). The co-expression patterns of *ABC1 family protein* with *CYP97A3* and *EMB1144* with *LYC* suggest that these genes may also play potential roles in terpenoid accumulation. Therefore, the transcriptome-based analysis provides a basis for identifying candidate genes involved in multiple metabolic pathways and reveals the coordinated transcriptional regulation underlying floral scent formation in *S. oblata*.

### *3.10. Validation of Candidate Gene Expression by qRT-PCR*

To validate the reliability of the transcriptome data, three candidate genes associated with floral aroma formation were selected for qRT-PCR analysis, including *LYC*, *LTPG1*, and *LOX6*. These genes were selected because they were associated with carotenoid metabolism, volatile transport, and fatty acid lipoxygenase metabolism, respectively. The qRT-PCR analysis was performed using petal samples from four developmental stages (S1–S4), and the expression patterns were compared with the RNA-seq data. Overall, the qRT-PCR results were largely consistent with the expression trends observed in the transcriptome data, confirming the reliability of the transcriptome analysis (Figure 15).

(**A**)

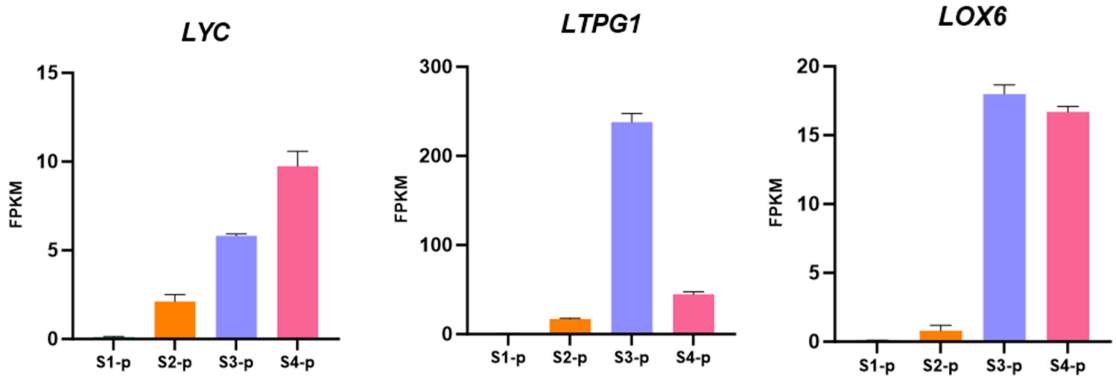



**Figure 15.** *Cont.*

(**B**)

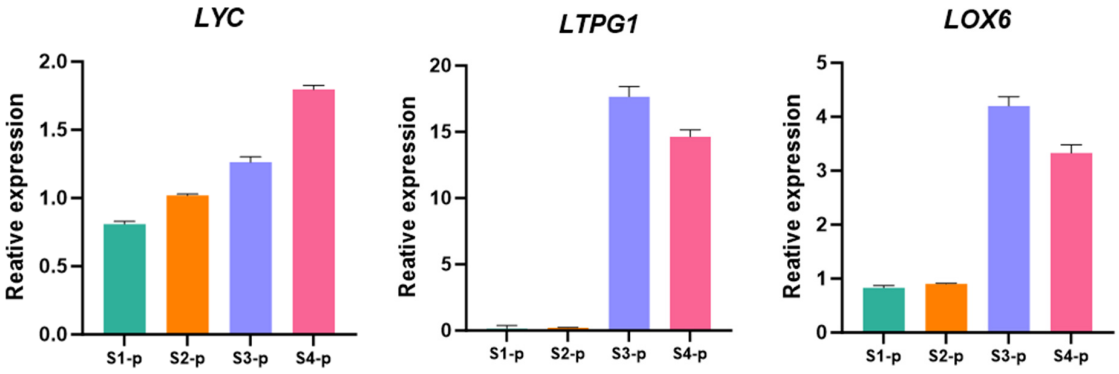



**Figure 15.** qRT-PCR validation of candidate genes related to floral aroma formation in *S. oblata*. (**A**) RNA-seq FPKM values of three candidate genes (*LYC*, *LTPG1*, and *LOX6*) at four petal developmental stages (S1–S4). (**B**) Relative expression levels of the three candidate genes at the corresponding stages measured by qRT-PCR. Note: Data are presented as means ± SD of three biological replicates. Actin was used as the internal control for qRT-PCR.

## 4. Discussion

### *4.1. Floral Aroma Emission Characteristics of S. oblata*

Floral volatile emission is a critical determinant of the ornamental value of *S. oblata* [45], and this sensory trait is governed by volatile secondary metabolites [46]. Although *S. oblata* is a well-known aromatic woody plant, the mechanisms underlying its aroma formation and emission remain incompletely understood.

The dynamic changes in VOC emission during flowering follow general patterns shared with other aromatic woody plants, yet exhibit species-specific timing. In *S. oblata*, VOC levels in petals increased markedly at the full-bloom stage, consistent with the majority of *Syringa* cultivars, which typically show the greatest VOC diversity and abundance at full bloom [47]. Similar patterns have been observed in *Syringa pekinensis*, where total VOCs peaked at full bloom and the proportion of alcohols increased during late flowering [48]. By contrast, *hybrid Luculia* reaches its aroma peak at the initial flowering stage and declines thereafter [38], highlighting interspecific variation in emission dynamics. The volatile oil content in *S. oblata* flowers is higher than that in leaves, and floral extracts contain more complex components [49].

In the present study, compound-level metabolomic profiling revealed that petals were the major floral organs contributing to VOC accumulation, and the full-bloom stage represented the critical period for aroma emission. Based on rOAV evaluation and multivariate screening, seven VOCs were identified as the predominant aroma-active compounds in *S. oblata* petals: (E)-β-damascone, (E)-2-nonenal, 2-nonenal, (E,Z)-2,6-nonadienal, (E,E)-2,4-nonadienal, α,α,4-trimethyl-3-cyclohexene-1-methanethiol, and (2E,6Z)-2,6-nonadien-1-ol. These compounds belong to three major chemical classes: terpenoid/carotenoid-derived volatiles, lipid-derived aldehydes and alcohols, and sulfur-containing compounds. This chemical distribution is broadly consistent with the general categories known to contribute to floral aroma in many ornamental plants [50,51].

The aroma profile of *S. oblata* also exhibited clear species specificity. In the *Oleaceae* family, sweet osmanthus (*Osmanthus fragrans*) is characterized by strong contributions of β-ionone and linalool [52], whereas *S. oblata* in this study showed a profile dominated by (E)-β-damascone together with C9 aldehydes and alcohols. Notably, both β-ionone and (E)-β-damascone originate from carotenoid-derived aroma metabolism, and carotenoid cleavage has been experimentally linked to ionone formation in *O. fragrans* via OfCCD1, suggesting that related enzymatic machineries may also operate in *S. oblata*.

Compared with the reported aroma profiles of lotus (*Nelumbo nucifera*) and wintersweet (*Chimonanthus praecox*) [1,10], *S. oblata* is distinguished by the prominent contribution of (E)-β-damascone and several C9 aldehydes and alcohols. Some of these key compounds are shared with other plant species: β-damascone is a major constituent of rose perfume [53]; both β-damascone and (E,Z)-2,6-nonadienal have been identified as key VOCs in tea trichomes and leaves [54]; β-damascone and (E,E)-2,4-nonadienal contribute to the aroma of Keemun black tea [26]; and β-damascone together with (E)-2-nonenal occurs in cooked carrots [55]. These cross-species comparisons suggest that while *S. oblata* shares common volatile biosynthetic routes with other aromatic plants, its unique combination and relative abundance of specific aroma-active compounds define its distinct fragrance character.

Overall, these results demonstrate that *S. oblata* possesses a distinct floral aroma profile, with petals at the full-bloom stage serving as the primary site of VOC production and emission. The dominance of (E)-β-damascone and C9 aldehydes/alcohols distinguishes *S. oblata* from other aromatic woody plants and provides a foundation for further investigations into the biosynthetic pathways and regulatory mechanisms underlying its floral aroma.

### *4.2. Biological Significance of Key VOCs*

The key VOCs in *S. oblata* not only determine its characteristic aroma but also provide important insights into their ecological functions through cross-species comparisons. These compounds hold potential biological significance in plant–pollinator interactions and stress responses.

Regarding pollinator attraction and chemical communication, C9 aldehydes such as (E)-2-nonenal, (E,Z)-2,6-nonadienal, and (E,E)-2,4-nonadienal have been shown to regulate insect behavior in various plant species. Research indicates that (E)-2-nonenal is a strong oviposition attractant for the diamondback moth (*Plutella xylostella*); in dual-choice oviposition experiments, plants treated with this compound received significantly more eggs than the control group [56]. (E,Z)-2,6-Nonadien-1-ol, a reduction product of the lipoxygenase pathway, is widely used as a key VOC in melon flavors owing to its intense "cucumber-like, green leaf" odor [7]. β-damascone, a characteristic product of the carotenoid cleavage pathway, possesses an odor profile highly conserved among various entomophilous plants in the *Rosaceae* and Oleaceae families. It has been confirmed to exhibit broad-spectrum attractive activity toward pollinators such as bees and hoverflies [57]. α,α,4-Trimethyl-3-cyclohexene-1-methanethiol is a monoterpene thiol known for its extremely low olfactory threshold [58]. Its detection in *S. oblata* petals, with a remarkably high rOAV of $1.13 \times 10^6$, suggests a potential role in attracting specific pollinator groups with sensitive olfaction.

In terms of stress response and adaptive protection, the present study does not demonstrate the ecological functions of these VOCs; however, the chemical identities and developmental accumulation patterns of the key compounds provide useful clues. Several key aldehydes identified in *S. oblata*, including (E)-2-nonenal, 2-nonenal, and (E,E)-2,4-nonadienal, are lipid-derived volatiles that can be associated with the fatty acid-lipoxygenase pathway. Green leaf volatiles, especially C6 and C9 aldehydes, alcohols, and esters, are generally formed from polyunsaturated fatty acids through LOX- and HPL-mediated reactions and are widely involved in plant defense, plant–plant communication, and plant–insect interactions [59,60]. In this study, the accumulation of these aldehydes at the full-bloom stage suggests that lipid-derived volatile metabolism may contribute not only to the green and fatty notes of *S. oblata* floral aroma but also to the physiological state of petals during peak aroma emission. Similarly, (E)-β-damascone is a carotenoid-derived aroma compound with a high odor contribution, but its ecological role in *S. oblata* should be interpreted cautiously. Its high rOAV supports its importance in human-perceived aroma, whereas its potential roles in pollinator attraction, photooxidative stress mitigation, or

pathogen defense require further validation through pollinator behavioral assays, oxidative stress measurements, and antimicrobial experiments. Thus, the key VOCs identified in *S. oblata* provide hypotheses for ecological function rather than experimental proof.

In summary, the key VOCs of *S. oblata* not only form the material basis of its characteristic aroma but also possess multiple ecological functions, including pollinator attraction, mitigation of photooxidative stress, and defense against pathogens.

### *4.3. Biological Significance of Carotenoid-Derived Compounds and Their Associated Genes*

In this study, integrative metabolomic and transcriptomic analysis identified *CYP97A3* and *LYC* as candidate genes potentially associated with the accumulation of the key aroma volatile β-damascone in *S. oblata*.

*CYP97A3* encodes a carotenoid β-ring hydroxylase (LUT5) involved in lutein biosynthesis in Arabidopsis thaliana [61]. Orthologs of *CYP97A3* regulate carotenoid composition and pigmentation in various plants [62–65]. In the present study, *CYP97A3* was up-regulated during the peak period of aroma emission and positively associated with (E)-β-damascone levels. *LYC* (lycopene β-cyclase) catalyzes the cyclization of lycopene to β-carotene, a precursor for β-branch carotenoids [66]. Notably, *CYP97A3* and *LYC* displayed opposite expression trends during petal development, suggesting possible substrate competition or regulatory balance between different carotenoid branches. Because we did not measure carotenoid intermediates or enzyme activity, these genes should be regarded as indirect candidates that may influence the availability of volatile precursors by modulating carotenoid metabolic balance.

Carotenoid-derived compounds also possess significant biological functions. Through cleavage by CCDs, carotenoids generate apocarotenoids and C13-norisoprenoids such as β-damascone, which have low odor thresholds and play ecological roles in pollinator attraction, plant defense, and environmental interactions [67,68]. In sweet osmanthus (*Osmanthus fragrans*), OfCCD1 has been shown to cleave carotenes to produce α-ionone and β-ionone, demonstrating that the carotenoid cleavage pathway participates in floral aroma formation in woody plants [68]. Thus, the carotenoid pathway has a dual role in flowers: it affects pigment accumulation and color expression, and generates volatile derivatives that shape floral aroma.

In *S. oblata*, flower color is primarily determined by anthocyanins [12], but the key aroma volatile (E)-β-damascone likely originates from carotenoid degradation. The candidate genes *CYP97A3* and *LYC* are both involved in carotenoid synthesis and transformation [69,70], raising the possibility that flower color and floral aroma may be coupled through upstream allocation of metabolic resources, precursor competition, and transcriptional regulation. Several lines of indirect evidence support this hypothesis: β-damascone is linked to carotenoid-derived metabolism; *CYP97A3* and *LYC* show antagonistic expression patterns suggesting dynamic regulation of metabolic flux; and the accumulation of volatiles and expression of metabolism-related DEGs show coordinated developmental changes, increasing at S2–S3 and declining at S4. These findings are consistent with previous reports that floral pigments and aroma compounds share biosynthetic pathways [71] and that pigment accumulation and aroma emission can change coordinately during flower development [72]. Nevertheless, because petal pigments were not quantified, the color-aroma relationship remains a regulatory hypothesis rather than a confirmed mechanism.

Understanding the formation mechanism of carotenoid-derived volatiles in *S. oblata* is important for revealing the molecular basis of color-aroma co-regulation in woody aromatic plants and provides a theoretical foundation for breeding new cultivars with attractive flower color and stable fragrance. Future research should simultaneously measure

carotenoid and anthocyanin contents across developmental stages and functionally validate the roles of *CYP97A3* and *LYC* in both pigment and volatile accumulation.

### *4.4. Limitations and Future Perspectives*

In this study, an integrated analysis of volatile metabolomics and transcriptomics elucidated the origin and emission patterns of floral aroma in *S. oblata*. However, certain limitations remain to be addressed in future research. The influence of environmental factors on aroma formation has not been thoroughly investigated, and the functional roles of key candidate genes remain to be validated through genetic experiments. Therefore, subsequent studies will focus on investigating the interactive effects between floral aroma and environmental factors of *S. oblata*, as well as validating the regulatory functions of target genes in VOC biosynthesis. This will provide a more robust molecular basis for the genetic improvement of floral aroma traits in *S. oblata*.

## 5. Conclusions

This study integrated volatile metabolomics and transcriptomics to characterize the floral aroma profile and potential regulatory mechanisms of *S. oblata* during flower development. The results showed that petals were the major floral organs contributing to aroma accumulation, and the full-bloom stage was the key period for VOC emission. Seven aroma-active VOCs, represented by β-damascone and several aldehydes and alcohols, were identified as the main contributors to the characteristic floral aroma of *S. oblata*. Transcriptome analysis further showed that differentially expressed genes during petal development were mainly enriched in metabolic pathways and the biosynthesis of secondary metabolites, and their expression patterns were generally consistent with the dynamic changes in VOC accumulation. Integrative analysis suggested that carotenoid pathway-related genes, especially *CYP97A3* and *LYC*, may be associated with the formation of carotenoid-derived aroma compounds, while genes related to fatty acid metabolism, volatile transport, and transcriptional regulation may also participate in floral aroma formation. These findings provide a molecular basis for understanding the origin of lilac fragrance and offer candidate gene resources for future improvement of aroma traits in *S. oblata*. Further functional validation, including targeted metabolite analysis, enzyme assays, and gene functional studies, will be necessary to confirm the regulatory roles of these candidate genes.

**Supplementary Materials:** The following supporting information can be downloaded at: https://www.mdpi.com/article/10.3390/horticulturae12070814/s1, Table S1: GC-MS results; Table S2: 121 terpenoid compounds; Table S3: complete rOAV dataset; Table S4: DEGs dataset.

**Author Contributions:** Y.T. conceived the idea of the study; X.W. and X.D. analyzed the data; Y.T., X.W. and X.D. interpreted the results; and P.X., S.B., Y.-e.B. and W.B. helped with discussion; Y.T. and X.W. wrote the paper; Y.T., X.W., X.D.,P.X., S.B., Y.-e.B. and W.B. made great contributions to manuscript preparation. All authors have read and agreed to the published version of the manuscript.

**Funding:** This research was funded by the National Natural Science Foundation of China under Grant No. 32560386; the Inner Mongolia Natural Science Foundation of China (Grant No. 2024MS03069); and the Basic Research Fund Project of Universities Directly under the Inner Mongolia Autonomous Region (Grant No. BR230144).

**Data Availability Statement:** Data will be made available on request.

**Acknowledgments:** We thank Inner Mongolia Agricultural University Forestry Experimental Center platform of China for providing technical support.

**Conflicts of Interest:** Author Peng Xie is employed by the Landscape Architecture Construction Service Center of Hohhot. The remaining authors declare that the research was conducted in the absence of any commercial or financial relationships that could be construed as a potential conflict of interest.

## References


1. Chen, L.; Song, H.; Xin, J.; Cheng, W.; Yang, M.; Sun, H. Unraveling the floral aroma of lotus (*Nelumbo nucifera*): Insights from volatile metabolomics and transcriptomics. *Ind. Crops Prod.* **2025**, *227*, 120782. [CrossRef]
2. Tu, M.; Liu, N.; He, Z.-S.; Dong, X.-M.; Gao, T.-Y.; Zhu, A.; Yang, J.-B.; Zhang, S.-B. Integrative omics reveals mechanisms of biosynthesis and regulation of floral scent in *Cymbidium tracyanum*. *Plant Biotechnol. J.* **2025**, *23*, 2162–2181. [CrossRef]
3. Lo, M.M.; Benfodda, Z.; Molinié, R.; Meffre, P. Volatile organic compounds emitted by flowers: Ecological roles, production by plants, extraction, and identification. *Plants* **2024**, *13*, 417. [CrossRef] [PubMed]
4. Wen, Y.; Pan, Y.L.; Yan, Q.; Zhao, P.; Li, Q. Research Progress on the Health Benefits of Forest Volatile Organic Compounds. *World For. Res.* **2017**, *30*, 19–23.
5. Duan, Y.; Lv, B.; Zhang, C.; Shi, L.; Li, J.; Liu, Y.; Chen, Q. Antibacterial activity of the biogenic volatile organic compounds from three species of bamboo. *Front. Plant Sci.* **2024**, *15*, 1474401. [CrossRef] [PubMed]
6. Zhou, F.; Pichersky, E. More is better: The diversity of terpene metabolism in plants. *Curr. Opin. Plant Biol.* **2020**, *55*, 1–10. [CrossRef] [PubMed]
7. Schwab, W.; Davidovich-Rikanati, R.; Lewinsohn, E. Biosynthesis of plant-derived flavor compounds. *Plant J.* **2008**, *54*, 712–732. [PubMed]
8. Ramya, M.; An, H.R.; Baek, Y.S.; Reddy, K.E.; Park, S.H. Orchid floral volatiles: Biosynthesis genes and transcriptional regulations. *Sci. Hortic.* **2018**, *235*, 62–69. [CrossRef]
9. Hernández, M.L.; Jiménez-López, J.; Cejudo, F.J.; Pérez-Ruiz, J.M. 2-Cys peroxiredoxins contribute to thylakoid lipid unsaturation by affecting ω-3 fatty acid desaturase 8. *Plant Physiol.* **2024**, *195*, 2152–2166. [CrossRef]
10. Shang, J.; Tian, J.; Cheng, H.; Yan, Q.; Li, L.; Jamal, A.; Xu, Z.; Xiang, L.; Saski, C.A.; Jin, S.; et al. The chromosome-level wintersweet (*Chimonanthus praecox*) genome provides insights into floral scent biosynthesis and flowering in winter. *Genome Biol.* **2020**, *21*, 200. [CrossRef] [PubMed]
11. Wang, R.; Shu, P.; Zhang, C.; Zhang, J.; Chen, Y.; Zhang, Y.; Du, K.; Xie, Y.; Li, M.; Ma, T.; et al. Integrative analyses of metabolome and genome-wide transcriptome reveal the regulatory network governing flavor formation in kiwifruit (*Actinidia chinensis*). *New Phytol.* **2021**, *233*, 373–389. [PubMed]
12. Han, M.; Lu, R.; Liu, C.; Zhao, S.; Du, F.; Yang, X.; Zhen, Z.; Chen, X. Multi-omics analysis revealed the difference in pigment accumulation profiles between *Syringa oblata* and *S. oblata* var. *alba*. *Sci. Hortic.* **2024**, *337*, 113467. [CrossRef]
13. Cui, L.; Hu, M.; Cao, P.; Niu, Y.; Li, C.; Liu, Z.; Kang, W. Chemical constituents and coagulation activity of Syringa oblata Lindl flowers. *BMC Chem.* **2019**, *13*, 108. [CrossRef] [PubMed]
14. Wang, Q.; Shen, J.; Wang, H.; Zeng, B.; Wang, W. Determination of odor-active compounds from *Phoebe neurantha* (Hemsl.) Gamble and *Osmanthus fragrans* (Thunb.) Lour. by GC–MS/O and micro-chamber combined with Tenax TA and multi-bed tubes. *Wood Sci. Technol.* **2021**, *55*, 1025–1041.
15. Bera, P.; Kotamreddy, J.N.R.; Samanta, T.; Maiti, S.; Mitra, A. Inter-specific variation in headspace scent volatiles composition of four commercially cultivated jasmine flowers. *Nat. Product Res.* **2015**, *29*, 1328–1335. [CrossRef]
16. Yang, F.Y.; Yang, S.; Wang, S.H.; Zhao, Y.; Liu, B. Comparative Analysis of Volatile Constituents in Three Lilac Flower Essential Oils. *Chemistry* **2019**, *82*, 1038–1042.
17. Oh, S.Y.; Shin, H.D.; Kim, S.J.; Hong, J. Rapid determination of floral aroma compounds of lilac blossom by fast gas chromatography combined with surface acoustic wave sensor. *J. Chromatogr. A* **2008**, *1183*, 170–178. [CrossRef] [PubMed]
18. *GB 23200.8-2016*; National Food Safety Standard—Determination of 500 Pesticides and Related Chemical Residues in Fruits and Vegetables—Gas Chromatography-Mass Spectrometry. Standards Press of China: Beijing, China, 2016.
19. Ji, C.; Guan, S.; Liu, C.; Yu, C.; Yao, Z.; Wan, H.; Ye, Q.; Zhou, G.; Wang, H.; Cheng, Y. Detection and analysis of VOCs in chili pepper based on HS-SPME-GC × GC-TOFMS and HS-SPME-GC-MS techniques. *Veg. Res.* **2024**, *4*, e021.
20. Yang, M.; Zhou, H.; Hu, X.; Liu, X.; Lei, J.; Ye, K.; Zhou, T.; Hu, J.; He, B. Untargeted metabolomics based on HS-SPME-GC-MS revealing the dynamic evolution of aroma components during cigar aging. *Front. Plant Sci.* **2025**, *16*, 1657415. [PubMed]
21. Yuan, H.; Cao, G.; Hou, X.; Huang, M.; Du, P.; Tan, T.; Zhang, Y.; Zhao, C.; Shen, L.; Liu, X.; et al. Development of a widely targeted volatilomics method for profiling volatilomes in plants. *Mol. Plant* **2022**, *15*, 189–202. [CrossRef] [PubMed]
22. Yuan, H.; Jiangfang, Y.; Liu, Z.; Su, R.; Li, Q.; Fang, C.; Huang, S.; Liu, X.; Fernie, A.R.; Luo, J. WTV2.0: A high-coverage plant volatilomics method with a comprehensive selective ion monitoring acquisition mode. *Mol. Plant* **2024**, *17*, 972–985. [CrossRef] [PubMed]

23. Huang, D.; Chen, X.; Tan, R.; Wang, H.; Jiao, L.; Tang, H.; Zong, Q.; Mao, Y. A comprehensive metabolomics analysis of volatile and non-volatile compounds in matcha processed from different tea varieties. *Food Chem. X* **2024**, *21*, 101234. [CrossRef] [PubMed]
24. Jiang, H.; Zhang, M.; Ye, J.; Qian, M.; Li, X.; Zhao, W.; Bai, W. HS-SPME-GC-MS and OAV analyses of characteristic volatile flavour compounds in salt-baked drumstick. *LWT—Food Sci. Technol.* **2022**, *170*, 114041.
25. Fang, X.; Xu, W.; Jiang, G.; Sui, M.; Xiao, J.; Ning, Y.; Niaz, R.; Wu, D.; Feng, X.; Chen, J.; et al. Monitoring the dynamic changes in aroma during the whole processing of Qingzhuan tea at an industrial scale: From fresh leaves to finished tea. *Food Chem.* **2023**, *439*, 137810. [CrossRef] [PubMed]
26. Huang, W.; Fang, S.; Wang, J.; Zhuo, C.; Luo, Y.; Yu, Y.; Li, L.; Wang, Y.; Deng, W.W.; Ning, J. Sensomics analysis of the effect of the withering method on the aroma components of Keemun black tea. *Food Chem.* **2022**, *395*, 133549. [CrossRef] [PubMed]
27. Xue, J.; Liu, P.; Yin, J.; Wang, W.; Zhang, J.; Wang, W.; Le, T.; Ni, D.; Jiang, H. Dynamic changes in volatile compounds of shaken black tea during its manufacture by GC × GC–TOFMS and multivariate data analysis. *Foods* **2022**, *11*, 1228. [CrossRef] [PubMed]
28. Yang, Y.; Ai, L.; Mu, Z.; Liu, H.; Yan, X.; Ni, L.; Zhang, H.; Xia, Y. Flavor compounds with high odor activity values (OAV > 1) dominate the aroma of aged Chinese rice wine (Huangjiu) by molecular association. *Food Chem.* **2022**, *383*, 132370. [CrossRef] [PubMed]
29. Chen, Y.; Zhang, R.; Song, Y.; He, J.; Sun, J.; Bai, J.; An, Z.; Dong, L.; Zhan, Q.; Abliz, Z. RRLC-MS/MS-based metabonomics combined with in-depth analysis of metabolic correlation network: Finding potential biomarkers for breast cancer. *Analyst* **2009**, *134*, 2003–2011. [PubMed]
30. Love, M.I.; Huber, W.; Anders, S. Moderated estimation of fold change and dispersion for RNA-seq data with DESeq2. *Genome Biol.* **2014**, *15*, 550. [CrossRef] [PubMed]
31. Varet, H.; Brillet-Guéguen, L.; Coppée, J.-Y.; Dillies, M.-A. SARTools: A DESeq2- and EdgeR-based R pipeline for comprehensive differential analysis of RNA-seq data. *PLoS ONE* **2016**, *11*, e0157022. [PubMed]
32. Mostafa, S.; Wang, Y.; Zeng, W.; Jin, B. Floral scents and fruit aromas: Functions, compositions, biosynthesis, and regulation. *Front. Plant Sci.* **2022**, *13*, 860157. [CrossRef] [PubMed]
33. Li, J.; Yu, X.; Shan, Q.; Shi, Z.; Li, J.; Zhao, X.; Chang, C.; Yu, J. Integrated volatile metabolomic and transcriptomic analysis provides insights into the regulation of floral scents between two contrasting varieties of Lonicera japonica. *Front. Plant Sci.* **2022**, *13*, 989036. [CrossRef] [PubMed]
34. Liu, G.; Huang, L.; Lian, J. Alcohol acyltransferases for the biosynthesis of esters. *Biotechnol. Biofuels Bioprod.* **2023**, *16*, 93. [CrossRef] [PubMed]
35. Li, Z.; Ahn, T.K.; Avenson, T.J.; Ballottari, M.; Cruz, J.A.; Kramer, D.M.; Bassi, R.; Fleming, G.R.; Keegstra, K.; Niyogi, K.K. Lutein accumulation in the absence of zeaxanthin restores nonphotochemical quenching in the Arabidopsis thaliana npq1 mutant. *Plant Cell* **2009**, *21*, 1798–1812. [CrossRef] [PubMed]
36. Brück, F.M.; Brummel, M.; Schuch, R.; Spener, F. In-vitro evidence for feed-back regulation of β-ketoacyl-acyl carrier protein synthase III in medium-chain fatty acid biosynthesis. *Planta* **1996**, *198*, 271–278.
37. Kazaz, S.; Barthole, G.; Domergue, F.; Ettaki, H.; To, A.; Vasselon, D.; De Vos, D.; Belcram, K.; Lepiniec, L.; Baud, S. Differential Activation of Partially Redundant Δ9 Stearoyl-ACP Desaturase Genes Is Critical for Omega-9 Monounsaturated Fatty Acid Biosynthesis During Seed Development in Arabidopsis. *Plant Cell* **2020**, *32*, 3613–3637. [CrossRef] [PubMed]
38. Du, P.; Deng, Q.; Wang, W.; Garg, V.; Lu, Q.; Huang, L.; Wang, R.; Li, H.; Huai, D.; Chen, X.; et al. scRNA-seq Reveals the Mechanism of Fatty Acid Desaturase 2 Mutation to Repress Leaf Growth in Peanut (*Arachis hypogaea* L.). *Cells* **2023**, *12*, 2305. [PubMed]
39. Grebner, W.; Stingl, N.E.; Oenel, A.; Mueller, M.J.; Berger, S. Lipoxygenase6-dependent oxylipin synthesis in roots is required for abiotic and biotic stress resistance of Arabidopsis. *Plant Physiol.* **2013**, *161*, 2159–2170. [CrossRef] [PubMed]
40. Toporkova, Y.Y.; Smirnova, E.O.; Mukhtarova, L.S.; Gorina, S.S.; Grechkin, A.N. Catalysis by allene oxide synthases (CYP74A and CYP74C): Alterations by the Phe/Leu mutation at the SRS-1 region. *Phytochemistry* **2020**, *169*, 112152. [PubMed]
41. Dai, Z.; Dong, H.; Zhang, Y.; Li, Y. Elucidating the contributions of multiple aldehyde/alcohol dehydrogenases to butanol and ethanol production in *Clostridium acetobutylicum*. *Sci. Rep.* **2016**, *6*, 28189. [CrossRef] [PubMed]
42. Lee, S.B.; Go, Y.S.; Bae, H.J.; Park, J.H.; Cho, S.H.; Cho, H.J.; Lee, D.S.; Park, O.K.; Hwang, I.; Suh, M.C. Disruption of glycosylphosphatidylinositol-anchored lipid transfer protein gene altered cuticular lipid composition, increased plastoglobules, and enhanced susceptibility to infection by the fungal pathogen *Alternaria brassicicola*. *Plant Physiol.* **2009**, *150*, 42–54. [CrossRef] [PubMed]
43. Adhikari, P.B.; Han, J.Y.; Ahn, C.H.; Choi, Y.E. Lipid Transfer Proteins (AaLTP3 and AaLTP4) Are Involved in Sesquiterpene Lactone Secretion from Glandular Trichomes in *Artemisia annua*. *Plant Cell Physiol.* **2019**, *60*, 2826–2836. [PubMed]
44. Chen, Y.; Zhang, H.; Zhang, M.; Zhang, W.; Ou, Z.; Peng, Z.; Fu, C.; Zhao, C.; Yu, L. Salicylic Acid-Responsive Factor TcWRKY33 Positively Regulates Taxol Biosynthesis in Taxus chinensis in Direct and Indirect Ways. *Front. Plant Sci.* **2021**, *12*, 697476. [PubMed]

45. Zheng, J.; Hu, Z.; Guan, X.; Dou, D.; Bai, G.; Wang, Y.; Guo, Y.; Li, W.; Leng, P. Transcriptome analysis of Syringa oblata Lindl. inflorescence identifies genes associated with pigment biosynthesis and scent metabolism. *PLoS ONE* **2017**, *10*, e0142542.
46. Yan, J.W.; Ban, Z.J.; Lu, H.Y.; Li, D.P.; Poverenov, E.; Luo, Z.S.; Li, L. The aroma volatile repertoire in strawberry fruit: A review. *J. Sci. Food Agric.* **2018**, *98*, 4395–4402. [CrossRef] [PubMed]
47. Li, Y.; Ma, H.; Wan, Y.; Li, T.; Liu, X.; Sun, Z.; Li, Z. Volatile Organic Compounds Emissions from *Luculia pinceana* Flower and Its Changes at Different Stages of Flower Development. *Molecules* **2016**, *21*, 531. [CrossRef] [PubMed]
48. Liu, Y.L.; Jin, M.R.; Yao, R.H.; Chen, X.M.; Wang, Y. Analysis of Floral Aroma Components and Cluster Analysis of Eight Oleaceae Species. *For. Ecol. Sci.* **2021**, *36*, 179–188.
49. Yu, A.N.; Yang, X.Z. Chemical composition of the essential oil of fresh wild Syringa pubescens flowers from China. *Adv. Mater. Res.* **2012**, *581–582*, 15–18. [CrossRef]
50. Pichersky, E.; Gershenzon, J. The formation and function of plant volatiles: Perfumes for pollinator attraction and defense. *Curr. Opin. Plant Biol.* **2002**, *5*, 237–243. [CrossRef] [PubMed]
51. Pichersky, E.; Noel, J.P.; Dudareva, N. Biosynthesis of plant volatiles: Nature's diversity and ingenuity. *Science* **2006**, *311*, 808–811. [PubMed]
52. Cai, Z.F.; Chen, Y.Q.; Xu, X.L.; Zhang, X.X.; Dong, B. Dynamic Changes in VOC Emissions During Flowering in Four *Osmanthus fragrans* Cultivars. *J. Zhejiang AF Univ.* **2017**, *34*, 608–619.
53. Kodama, N.; Okada, H.; Hachisu, M.; Ando, M.; Ito, N.; Nagata, K.; Katagiri, M.; Yasuda, Y.; Hiroki, I.; Yashiro, T.; et al. A rose flavor compound activating the NRF2 pathway in dendritic cells ameliorates contact hypersensitivity in mice. *Front. Nutr.* **2023**, *10*, 1081263. [CrossRef] [PubMed]
54. Qi, D.; Lu, M.; Shi, Y.; Zhang, X.; Yue, L.; Jia, H.; Dong, C.; Liu, H.; Yuan, C. Volatile metabolomics highlights tea trichome's positive contribution to aroma and quality of white tea. *Curr. Res. Food Sci.* **2025**, *11*, 101179. [PubMed]
55. Buttery, R.G.; Takeoka, G.R. Cooked carrot volatiles. AEDA and odor activity comparisons. Identification of linden ether as an important aroma component. *J. Agric. Food Chem.* **2013**, *61*, 9063–9066. [CrossRef] [PubMed]
56. Carroll, M.J.; Schmelz, E.A.; Meagher, R.L.; Teal, P.E.A. Attraction of Spodoptera frugiperda larvae to volatiles from herbivore-damaged maize seedlings. *J. Chem. Ecol.* **2006**, *32*, 1911–1924. [CrossRef] [PubMed]
57. Knudsen, J.T.; Eriksson, R.; Gershenzon, J.B. Diversity and distribution of floral scent. *Bot. Rev.* **2006**, *72*, 1–120. [CrossRef]
58. Buettner, A.; Schieberle, P. Evaluation of key aroma compounds in hand-squeezed grapefruit juice (Citrus paradisi Macfayden) by quantitation and flavor reconstitution experiments. *J. Agric. Food Chem.* **2001**, *49*, 1358–1363. [CrossRef] [PubMed]
59. Hassan, M.N.; Zainal, Z.; Ismail, I. Green leaf volatiles: Biosynthesis, biological functions and their applications in biotechnology. *Plant Biotechnol. J.* **2015**, *13*, 727–739. [CrossRef]
60. Ameye, M.; Allmann, S.; Verwaeren, J.; Smagghe, G.; Haesaert, G.; Schuurink, R.C.; Audenaert, K. Green leaf volatile production by plants: A meta-analysis. *New Phytol.* **2018**, *220*, 666–683. [PubMed]
61. Kim, J.; DellaPenna, D. Defining the primary route for lutein synthesis in plants: The role of Arabidopsis carotenoid β-ring hydroxylase CYP97A3. *Proc. Natl. Acad. Sci. USA* **2006**, *103*, 3474–3479. [CrossRef] [PubMed]
62. Niu, G.; Guo, Q.; Wang, J.; Zhao, S.; He, Y.; Liu, L. Structural basis for plant lutein biosynthesis from α-carotene. *Proc. Natl. Acad. Sci. USA* **2020**, *117*, 14150–14157. [CrossRef] [PubMed]
63. Lv, M.-Z.; Chao, D.-Y.; Shan, J.-X.; Shi, M.; Gao, J.-P.; Lin, H.-X. Rice carotenoid β-ring hydroxylase CYP97A4 is involved in lutein biosynthesis. *Plant Cell Physiol.* **2012**, *53*, 987–1002. [CrossRef] [PubMed]
64. Stigliani, A.L.; Giorio, G.; D'Ambrosio, C. Characterization of P450 carotenoid β-and ε-hydroxylases of tomato and transcriptional regulation of xanthophyll biosynthesis in root, leaf, petal and fruit. *Plant Cell Physiol.* **2011**, *52*, 851–865. [PubMed]
65. Guo, P.; Huang, Y.; Jin, P.; Li, X.; Ma, Q.; Yu, L.; Zhao, W.; Wang, Y.; Shang, F. Combined transcriptomic and metabolomic analysis of the coloration mechanism in colored-leaf *Osmanthus fragrans* 'Jinyu Guihua'. *Plants* **2026**, *15*, 385. [CrossRef] [PubMed]
66. Cunningham, F.X.; Pogson, B.; Sun, Z.; McDonald, K.A.; DellaPenna, D.; Gantt, E. Functional analysis of the beta and epsilon lycopene cyclase enzymes of Arabidopsis reveals a mechanism for control of cyclic carotenoid formation. *Plant Cell* **1996**, *8*, 1613–1626. [CrossRef] [PubMed]
67. Dudareva, N.; Klempien, A.; Muhlemann, J.K.; Kaplan, I. Biosynthesis, function and metabolic engineering of plant volatile organic compounds. *New Phytol.* **2013**, *198*, 16–32. [CrossRef] [PubMed]
68. Baldermann, S.; Kato, M.; Kurosawa, M.; Kurobayashi, Y.; Fujita, A.; Fleischmann, P.; Watanabe, N. Functional characterization of a carotenoid cleavage dioxygenase 1 and its relation to carotenoid accumulation and volatile emission during floral development of *Osmanthus fragrans* Lour. *J. Exp. Bot.* **2010**, *61*, 2967–2977. [CrossRef] [PubMed]
69. Wang, H.R.; Zhang, R.R.; Wang, Y.H.; Zhou, J.H.; Sun, M.; Wang, L.X.; Zhang, Y.Q.; Liang, Y.; Li, X.J.; Xu, Z.S.; et al. Carotene hydroxylase DcCYP97A3 affects carotenoid metabolic flow and taproot color by influencing the conversion of α-carotene to lutein in carrot. *Hortic. Res.* **2025**, *12*, uhaf054. [PubMed]
70. Lu, S.; Zhang, Y.; Zhu, K.; Yang, W.; Ye, J.; Chai, L.; Xu, Q.; Deng, X. The citrus transcription factor CsMADS6 modulates carotenoid metabolism by directly regulating carotenogenic genes. *Plant Physiol.* **2018**, *176*, 2657–2676. [CrossRef] [PubMed]

71. Yeon, J.Y.; Kim, W.S. Biosynthetic linkage between the color and scent of flowers: A review. *Hortic. Sci. Technol.* **2021**, *39*, 697–713. [CrossRef]
72. Yeon, J.Y.; Kim, W.S. Positive correlation between color and scent in rose petals with floral bud development. *Hortic. Sci. Technol.* **2020**, *38*, 608–619. [CrossRef]

**Disclaimer/Publisher's Note:** The statements, opinions and data contained in all publications are solely those of the individual author(s) and contributor(s) and not of MDPI and/or the editor(s). MDPI and/or the editor(s) disclaim responsibility for any injury to people or property resulting from any ideas, methods, instructions or products referred to in the content.